JGP Journal of General Physiology

ARTICLE

Voltage-Gated Na Channels

Altered $Na_V1.9$ channel activity in two Tyr66Ser variant carriers with small fiber dysfunction

Noortje W.M. van den Braak[1,2], Samuel Kuehs[3], Greta Z. Peschke[1,2], Barbara Namer[1,4,5], Annette Lischka[1,6], Katja Eggermann[1,6], Christina Dumke[1,2], Vishal Sudha Bhagavath Eswaran[1,7], Stefan Nikolin[8], Joachim Weis[8], Jörg B. Schulz[2], Angelika Lampert[1,7], Ingo Kurth[1,6], Roman Rolke[1,9], Enrico Leipold[3], and Maike F. Dohrn[1,2]

Pain perception is a complex experience, the initiation of which is mediated, among others, by voltage-gated sodium channels. Pathogenic variants in the sodium channel gene *SCN11A* encoding for $Na_V1.9$ have been associated with various pain loss and neuropathic pain conditions. We herein describe the novel heterozygous *SCN11A* variant c.197A>C; p.(Tyr66Ser) that is absent in controls and cosegregates with small fiber neuropathy in a mother-and-son duo. To a variable degree, but progressively over time, both patients developed positive and negative sensory symptoms and milder autonomic signs. Upon quantitative sensory testing, we found significant thermal hypoesthesia and pinprick hyperalgesia in both individuals. Rectangle, half-sine-, and sine-wave stimulation applied to hands and feet in both individuals revealed signs of axonal on/off-like hyperexcitability, possibly due to continuous activation of CMi-fibers that are insensitive to mechanical stimulation (also known as sleeping nociceptors). Nerve conduction studies were unremarkable, whereas pain-related evoked potentials showed pathological responses in both individuals. The intraepidermal nerve fiber density was reduced at the index patient's distal leg. Patch-clamp analyses revealed that p.(Tyr66Ser) shifted both the voltage dependence of activation and steady-state inactivation of $Na_V1.9$ to more depolarized potentials, accompanied by accelerated deactivation and a slowdown of the channel's inactivation kinetics. In addition, overexpression of the variant in mouse sensory neurons shortened the duration of individual action potentials and enhanced action potentials after hyperpolarization. In this translational *n-of-two* study, we present longitudinal data on disease progression and provide functional evidence that the *SCN11A* variant p.(Tyr66Ser) is a strong candidate to contribute to the patients' phenotype.

Introduction

Small fiber neuropathies (SFN) are characterized by dysfunction and/or degeneration of thinly or unmyelinated Aδ- and C-fibers (Devigili et al., 2008). The most common symptom, neuropathic pain, is often described with a burning, stabbing, or electrifying character, and to be located right underneath or on the skin surface (Dohrn et al., 2022). Other sensory symptoms linked to SFN are categorized as positive (allodynia, dysesthesia, hyperesthesia, itch, or paresthesia) or negative (hypoesthesia for heat or light touch, numbness, no or reduced sensation of sharp stimuli) symptoms. Since Aδ- and C-nerve fibers do not innervate the skin only, but also internal organs through autonomic nerve fibers, other possible symptoms of SFN are dry eyes and/or mouth, reduced sweating, orthostatic dysfunction, or gastrointestinal symptoms.

CMi-fibers, also known as sleeping nociceptors, are a unique C-fiber subtype characterized by resistance to mechanical stimulation, by inability to follow electrical pulses delivered at higher frequencies, and by their distinctive affinity to sine-wave stimuli (Namer and Handwerker, 2009; Jonas et al., 2018; Werland et al., 2021). Spontaneous activity of these fibers has

[1]Scientific Center for Neuropathic Pain Aachen (SCN[AACHEN]), Uniklinik RWTH Aachen, Aachen, Germany; [2]Department of Neurology, Medical Faculty RWTH Aachen University, Aachen, Germany; [3]Department of Anesthesiology and Intensive Care and Center of Brain, Behavior and Metabolism, University of Lübeck, Lübeck, Germany; [4]Interdisciplinary Center for Clinical Research (IZKF), Medical Faculty RWTH Aachen University, Aachen, Germany; [5]Department of Anaesthesiology, Intensive Care, Emergency Medicine, Centre for Interdisciplinary Pain Medicine, University Hospital Wuerzburg, Würzburg, Germany; [6]Zentrum für Humangenetik und Genommedizin, Medical Faculty RWTH Aachen University, Aachen, Germany; [7]Institute for Neurophysiology, Uniklinik RWTH Aachen, Aachen, Germany; [8]Institute of Neuropathology, Medical Faculty RWTH Aachen University, Aachen, Germany; [9]Department of Palliative Medicine, Medical Faculty RWTH Aachen University, Aachen, Germany.

Correspondence to Maike F. Dohrn: mdohrn@ukaachen.de

This work is part of a special issue on voltage-gated sodium (Na_v) channels.

© 2025 van den Braak et al. This article is distributed under the terms as described at https://rupress.org/pages/terms102024/.

Check for updates

Downloaded from rupress.org/jgp/article-pdf/157/6/e202413691/1952150/jgp_202413691.pdf by guest on 15 November 2026

been identified as a functional correlate of neuropathic pain and small fiber dysfunction (Kleggetveit et al., 2012; Ochoa et al., 2005; Sauerstein et al., 2018). Transcutaneous electrical sine-wave stimulation of the skin effectively activates CMi-fibers (Jonas et al., 2018), whereas half-sine-wave stimuli predominantly activate CM-fibers, and rectangular electrical pulses target A-fibers (Rukwied et al., 2020). Given that small fiber dysfunction manifests as a complex and variable syndrome difficult to measure or quantify, psychophysical examinations such as axon stimulation have been of growing importance to build a bridge between other experimental strategies assessing nerve fiber function.

The etiology of SFN remains unknown in about 50% of cases (Devigili et al., 2008; de Greef et al., 2018; Peters et al., 2013). For those patients, this means that targeted disease-modifying treatments are far from sight. At the same time, it is not possible to counsel on disease progression, to prevent complications, or draw conclusions on prognosis. Genetic variants in genes and gene products linked to the initiation and modulation of pain perception are strong candidates to potentially explain a part of the "idiopathic" SFN cases. Voltage-gated sodium channels (Na_Vs) of sensory afferent fibers are essential for the initiation and propagation of action potentials that encode sensory information, including pain. Among the nine human Na_Vs(Na_V1.1–Na_V1.9), Na_V1.7 (*SCN9A*), Na_V1.8 (*SCN10A*), and Na_V1.9 (*SCN11A*) are the most abundantly expressed isoforms in Aδ- and C-nerve fibers (Dib-Hajj et al., 2010). While Na_V1.7 and Na_V1.8 are important for setting the action potential threshold and contribute most of the Na^+ inward current underlying the fast action potential upstroke in sensory neurons, Na_V1.9 channels are already active at subthreshold membrane potentials (Cummins et al., 1998; Herzog et al., 2003; Meents et al., 2019). Consequently, Na_V1.9 is suggested to amplify those subthreshold signals, ultimately facilitating the generation of action potentials (Leipold et al., 2015; Lolignier et al., 2015). Specifically, Na_V1.9 plays a crucial role in cold pain sensation and cold allodynia (Lolignier et al., 2015; Leipold et al., 2015). Rare pathogenic *SCN11A* variants have been associated with a spectrum of neuropathic pain disorders with symptoms ranging from congenital pain insensitivity (CIP) to extreme neuropathic pain conditions (Goodwin and McMahon, 2021). In addition to pain insufficiency, CIP symptoms include severe ulcerations, auto-mutilation, hyperhidrosis, and gastrointestinal disturbances (Lischka et al., 2022, 2023). *SCN11A* variants associated with CIP have, so far, all been located within the S6 segments lining the channel pore (Leipold et al., 2013; Phatarakijnirund et al., 2016; King et al., 2017). In contrast, other pathogenic *SCN11A* missense variants have been discussed in the context of familial episodic pain and painful peripheral neuropathy, associated with peripheral pain episodes of variable intensity, often accompanied by altered temperature thresholds and signs of small fiber dysfunction (Zhang et al., 2013; Huang et al., 2014; Leipold et al., 2015; Okuda et al., 2016; Han et al., 2017; Nagao et al., 2025). Since all experimentally validated *SCN11A* variants are heterozygous missense mutations, genotype–phenotype–function studies are of particular importance (Table S1). For example, the recently reported variant p.(Leu811Phe) has been associated with familial episodic pain, although it is located at the exact same position at the intracellular pore interface of Na_V1.9 as the CIP-related variant p.(Leu811Pro) (Nagao et al., 2025). Based on molecular dynamics simulations, it was hypothesized that the two variants may differentially affect the channel pore structure and, thus, the conformational transitions between conducting and nonconduction states, ultimately resulting in contrasting clinical phenotypes (Nagao et al., 2025).

We herein describe in-depth the clinical phenotype associated with the novel heterozygous *SCN11A* variant p.(Tyr66Ser), which we identified upon exome sequencing in a mother-and-son duo with SFN of otherwise unknown cause. In addition, we present longitudinal data on disease progression, use psychophysical methods to draw conclusions on nerve fiber activity patterns, and, using patch-clamp electrophysiology, demonstrate that p.(Tyr66Ser) affects activation and inactivation properties of Na_V1.9, suggesting a causal link between the variant and patient phenotype.

Materials and methods

Enrollment policy

Patients were recruited from our patient registry established through the Scientific Center for Neuropathic Pain Aachen (SCN^{AACHEN} total cohort, n = 295). We obtained the patients' written informed consent prior to study enrollment. The study protocol has been approved by the local institutional review board and conducted according to the Declaration of Helsinki. All patients were examined at the Neuromuscular Outpatient Clinic, Department of Neurology of the RWTH Aachen University Hospital in Aachen, Germany, prior to their inclusion in the registry. By inclusion criteria, we enrolled patients with SFN of hereditary or idiopathic etiology. SFN was confirmed following the Devigili criteria (Devigili et al., 2008), with a compatible clinical phenotype and additional signs of Aδ- or C-nerve fiber dysfunction on quantitative sensory testing (QST) and/or degeneration on skin biopsy, with large fiber polyneuropathy excluded by nerve conduction studies. We assessed other relevant differential diagnoses by patient history and laboratory work.

Clinical assessment of sensory and autonomic symptoms

We followed a standardized protocol for all study visits (Dohrn et al., 2022). Patients were examined by the same experienced investigators. Besides comorbidities, family history, prior and current medications, and autonomic symptoms, the patient history focused on sensory symptoms including a detailed pain assessment, using the numerical rating scale (NRS) with a range from 0 (no pain) to 10 (most severe pain) and the PainDETECT questionnaire (Freynhagen et al., 2016). A detailed bedside examination included perception of light touch, pinprick, and temperature, as well as large fiber signs, including reduced reflex levels, muscle strength, afferent ataxia, and reduced vibration perception. For the latter, we used a standardized 64-Hz Rydel–Seiffer tuning fork. Autonomic symptoms were assessed following a standardized checklist. To quantify orthostatic dysfunction, we measured blood pressure and heart rate at supine and standing position. Using a standardized electrochemical

Downloaded from rupress.org/jgp/article-pdf/157/6/e202413691/1952150/jgp_202413691.pdf by guest on 15 November 2026

skin impedance test (Sudoscan, Impeto Medical, France), we measured sweat production as a response to C-fiber stimulation at palms of the hands and soles of the feet. Absolute values were normalized using sex-, age-, and weight-matched controls (Smith et al., 2014).

Quantitative sensory testing

To determine small fiber dysfunction, we followed the standardized protocol for QST established by the German Research Network on Neuropathic Pain (Rolke et al., 2006). We assessed the clinically most affected hands and feet of the mother-and-son duo and compared them with published sex-, age-, and site-related reference data (Magerl et al., 2010) for normalization and the calculation of z-values. Pain was rated on the detailed NRS from 0 to 100, with 100 representing the most intense pain imaginable and 0 no pain or imperceptible stimulus.

Pain-evoked potentials

Pain-related evoked potentials (PREPs) have become an established method to assess peripheral Aδ-fiber function and central processing pathways (Siedler et al., 2020). SFN has been associated with reduced peak-to-peak amplitudes, whereas demyelinating neuropathy is reflected by prolonged latencies (Siedler et al., 2020). Using a concentric planar electrode (Inomed), we stimulated at the clinically most affected hand and foot dorsum of the mother-and-son duo. We applied a standardized protocol (Hansen et al., 2015) for all measurements, generating electrical stimuli using a Digitimer DS7A connected to a trigger unit. The recording of cortical potentials was performed using an electroencephalography surface electrode placed over Cz according to the international 10–20 system. Linked ear electrodes were used as reference electrodes. We recorded 40 averaged (per body site) potentials from the scalp. Recordings were performed using the 32-channel BrainAmp DC amplifier system, including the BrainVision Recording software. We analyzed amplitudes and latencies of PREPs with BrainVision Analyzer software.

Axon stimulation

To assess pain responses upon electrical pulses applied to the skin (Jonas et al., 2018), we stimulated the two patients and 20 healthy controls at the volar arm and foot dorsum. Three stimulation forms (rectangular, half-sinusoidal, and sinusoidal) with varying currents (amperages) and frequencies were performed, as well as a one-min sinusoidal stimulation, followed by laser Doppler imaging to detect axon reflex erythema. Pain was rated on the detailed NRS from 0 to 100, with 100 representing the most intense pain imaginable and 0 no pain or imperceptible stimulus. Stimuli were generated using two constant current stimulators (rectangular: Digitimer DS7A; half-sinusoidal and sinusoidal: DS5) and a digital/analogue converter (NI USB-6221), controlled by the software DAPSYS8. We used a handheld customized bipolar platinum electrode (0.7 mm wire diameter, 1.5 mm contact surface length, 2 mm wire distance) to apply the electrical stimulation to the skin. Electrical rectangular stimulation was performed with 200-µs pulses (10 stimuli per cycle) at 4 Hz with currents of 1.0, 0.5, 2.0, 0.25, 4.0, and 3.0 mA. For frequency-dependent rectangular stimulation (10, 6, 50, 100, 20, 4 Hz), the current was set at the amplitude, which was rated 30 ± 5 on the NRS. Half-sinusoidal stimulation (500-ms pulse width, 1 stimulus per cycle) was applied at 0.2, 0.1, 0.4, 0.8, 0.6, and 1.0 mA. Sinusoidal stimulation was conducted with 10 stimuli per cycle, with amplitudes of 0.1, 0.05, 0.2, 0.025, 0.4, and 0.3 mA, at frequencies varying from 20, 4, 10, 100, 50, 6 Hz. The individual current setting for each participant to achieve a 30 ± 5 rating on the NRS was used during a 1-min sinusoidal stimulation (4 Hz, individual current setting), during which pain ratings were assessed before the start of the protocol and every 10 s during stimulation. Axon flare was measured using a laser Doppler imager (FLP-2; Moor Instruments) and analyzed with the MoorFLP-2 software. To minimize artifacts, we only evaluated pixels exceeding a defined flux threshold (baseline plus double SD). Axon flare size was calculated as the product of valid pixel counts and pixel size minus the baseline flare area.

Skin biopsies

To assess intraepidermal nerve fiber density (IENFD) as a marker of small fiber degeneration, we evaluated preexisting neuropathology reports requested for diagnostic purposes. The standards for obtaining, fixing, processing, and interpreting skin biopsies (Lauria's criteria) have been described elsewhere (Weis et al., 2011).

Molecular genetic sequencing

Exome sequencing was performed by the use of Illumina Enrichment Kit (Nextera Rapid Capture Exome v1.2). The generated library was sequenced on an Illumina NextSeq 500 sequencer. The generation of the analyzed "bam," "FastQ," and "vcf" files was carried out with the standard BWA pipeline (BWA Enrichment, version 2.1.0.0, Illumina, reference genome: hg19). The generated raw data were analyzed using the variant annotation software kggseq (v1, https://pmglab.top/kggseq/).

Multiple sequence alignment and structural visualization

The protein sequences for the 9 human Na_V subtypes were obtained from the UniProt database (Accession codes—hNa_v1.1, Q8NEY1; hNa_v1.2, Q99250; hNa_v1.3, Q9NY46; hNa_v1.4, P35499; hNa_v1.5, Q14524; hNa_v1.6, Q9UQD0; hNa_v1.7, Q15858; hNa_v1.8, Q9Y5Y9; and hNa_v1.9, Q9UI33). Multiple sequence alignment was performed using the T-Coffee package provided by JABAWS (Troshin et al., 2011) and shaded according to the level of conservation of the residues. Black shades represent fully conserved residues, gray shades represent partially conserved residues, and no shade represents nonconserved residues. The 3D structure of hNa_v1.9 was obtained from the AlphaFold Protein Structure Database (Varadi et al., 2024; Jumper et al., 2021; Identifier AF-Q9UI33-F1). The structure was downloaded and aligned vertically to a horizontal membrane bilayer using the PPM web server 3.0 (Lomize et al., 2022). Structural visualization of the p.(Tyr66Ser) residue and image generation were carried out using UCSF ChimeraX (Pettersen et al., 2021).

Isolation and transfection of mouse dorsal root ganglion neurons

Animal care and associated experimental procedures followed the guidelines established by the animal welfare committee of

Downloaded from rupress.org/jgp/article-pdf/157/6/e202413691/1952150/jgp_202413691.pdf by guest on 15 November 2026

the University of Luebeck. Dorsal root ganglia (DRG) from all levels of the spinal cord of 8- to 12-wk-old C57BL/6 wild type and homozygous $Na_V1.8/Na_V1.9$ double-knockout (DKO) mice lacking functional $Na_V1.8$ and $Na_V1.9$ channels (Alves-Simões et al., 2024) were extracted following a procedure described earlier (Dib-Hajj et al., 2009). Subsequently, isolated neurons were transfected by electroporation with cDNA expression constructs containing the coding sequence of either human $Na_V1.9$ or human $Na_V1.9$-Tyr66Ser together with a reporter cassette encoding the enhanced green fluorescent protein following an established protocol (Loose et al., 2023).

Electrophysiology

Voltage- and current-clamp recordings were obtained in the whole-cell configuration of the patch-clamp method using an EPC-10 patch-clamp amplifier operated by PatchMaster software (HEKA Elektronik). Patch pipettes were fabricated from Kimax borosilicate glass of about 1.0–2.5 MΩ resistance and coated with silicone adhesive (RTV 615; Momentive Performance Materials) to reduce tip capacitance. Series resistance was corrected electronically up to 85%, and all voltages were corrected for the liquid junction potential (−7 mV). The bath solution for voltage-clamp recordings contained (in mM) 130 NaCl, 2 KCl, 2.5 $CaCl_2$, 1 $MgCl_2$, 20 tetraethylammonium chloride (TEA-Cl), 10 HEPES (pH 7.4 with NaOH), and was supplemented with tetrodotoxin (TTX) (1 µM), $CdCl_2$ (100 µM), and 4-aminopyridine (1 mM) to block Na^+ currents, Ca^{2+} currents, and K^+ currents, respectively, endogenous in $Na_V1.8/Na_V1.9$ DKO DRG neurons. The patch pipette contained (in mM) 10 NaCl, 130 CsF, 10 EGTA, and 10 HEPES (pH 7.4 with CsOH). The bath solution for current-clamp recordings contained (in mM) 120 NaCl, 3 KCl, 2.5 $CaCl_2$, 1 $MgCl_2$, 30 HEPES, 15 glucose (pH 7.4 with NaOH), and the pipette, 125 KCl, 8 NaCl, 1 $CaCl_2$, 1 $MgCl_2$, 0.4 Na_2-GTP, 4 Mg-ATP, 10 EGTA, and 10 HEPES (pH 7.3 with KOH). All recordings were performed at a constant temperature of 20 ± 0.5°C using a microincubation stage (ALA Scientific Instruments) feedback-controlled by a PTC-10 temperature controller (NPI Electronic GmbH). Electrophysiological recordings were analyzed with FitMaster (HEKA Elektronik) and Igor Pro (WaveMetrics) software.

All voltage-clamp recordings were obtained using DKO DRG neurons that were transfected with plasmids encoding either human $Na_V1.9$ or human $Na_V1.9$-Tyr66Ser. The holding potential was set to −137 mV in all experiments. Data were low-pass filtered at 3 kHz and sampled at an interval of 40 µs. Leak and capacitive currents were recorded using a P/6 protocol with six leak pulses, each with 0.15 times the amplitude of the test pulse P. Summed and scaled leak traces were subtracted online using the leak pulse feature available in PatchMaster software.

Channel activation

Activation of Na_Vs was measured with test pulses ranging from −127 to 13 mV applied in steps of 10 mV every 10 s. The voltage dependence of channel activation was estimated from peak current densities using the following formalism:

$$\frac{I(V)}{C_m} = \Gamma \cdot (V - E_{rev}) \cdot P_{open}$$
$$P_{open} = \frac{1}{1 + e^{-(V-V_m)/k_m}} \quad (1)$$

with the cell membrane capacitance C_m, conductance density Γ, and the reversal potential E_{rev}. V_m is the half-maximal activation voltage and k_m the corresponding slope factor.

Activation and inactivation kinetics

The kinetics of activation and fast inactivation of $Na_V1.9$ and $Na_V1.9$-Tyr66Ser channels were analyzed between −47 and 3 mV with a model assuming one activation gate and one inactivation gate:

$$I(t) = I_0 \cdot m(t) \cdot h(t)$$
$$m(t) = 1 - e^{\left(-\frac{t}{\tau_m}\right)}$$
$$h(t) = h_\infty + (1 - h_\infty) \cdot e^{\left(-\frac{t}{\tau_h}\right)} \quad (2)$$

with the current amplitude I_0. $m(t)$ and $h(t)$ describing the kinetics of channel activation and inactivation, respectively, with the associated time constants τ_m and τ_h, and h_∞ characterizing the fraction of noninactivating current after infinite time.

Channel deactivation

Channels were activated with a 25-ms depolarization to −37 mV before deactivation was triggered by a 150-ms repolarization period at voltages ranging from −127 to −57 mV in steps of 10 mV, with a repetition interval of 10 s. The current decay during the repolarization period was fitted according to the following equation:

$$I(t) = I_0 - (I_0 - I_\infty) \cdot \left(1 - e^{-\frac{t}{\tau_d}}\right) \quad (3)$$

where I_0 is the maximal current amplitude and I_∞ the current remaining after infinite time. τ_d is the deactivation time constant. The voltage dependence of activation and deactivation time constants was described with a formalism assuming a one-step process for channel opening and closing:

$$\tau(V) = \tau_0 + \frac{1}{\alpha_0 \cdot \left[e^{\frac{(V-V_m)\cdot q\cdot\delta}{kT}} + e^{\frac{(V-V_m)\cdot q\cdot(1-\delta)}{kT}}\right]} \quad (4)$$

τ_0 is the voltage-independent, limiting speed of deactivation, α_0 is the rate at the equilibrium voltage V_m, and kT is the thermal energy. q is the total gating charge transfer, and δ is the symmetry factor specifying the gating charge fraction associated with channel activation.

Steady-state channel inactivation

Na_Vs were activated with a first 50-ms test pulse to −37 mV followed by a conditioning interval of 500 ms at voltages ranging from −147 to −7 mV in steps of 10 mV. Peak currents of not inactivated channels were measured in a subsequent 50-ms test pulse to −37 mV. The repetition interval was 10 s. The normalization

Downloaded from rupress.org/jgp/article-pdf/157/6/e202413691/1952150/jgp_202413691.pdf by guest on 15 November 2026

of the current amplitudes after conditioning ($I_{500\ ms}$) to the control current amplitude before conditioning (I_0) was described using the following Boltzmann formalism:

$$\frac{I_{500\,ms}(V)}{I_0} = h_{max} - (h_{max} - h_{min}) \cdot \left(\frac{1}{1 + e^{-(V - V_h)/k_h}}\right) \quad (5)$$

with the maximal and minimal channel availability h_{max} and h_{min}, the half-maximal inactivation voltage V_h, and the corresponding slope factor k_h.

Current-clamp recordings

All current-clamp recordings were obtained from wild type DRG neurons overexpressing either human $Na_V1.9$ or variant p.(Tyr66Ser). The resting membrane voltage of the neurons was measured by zero-current injection directly after establishing the whole-cell configuration. Single action potentials were evoked by injecting a current of 100–200 pA for a period of 10 ms, followed by a 200-ms period without current injection. Sampling interval for voltage measurements was 50 µs. Parameters characterizing individual action potentials, including action potential peak voltage (V_{peak}), minimum after-hyperpolarization voltage (V_{AHP}), voltage threshold of action potential firing (V_{th}), and action potential duration measured at a voltage of 0 mV ($Width_0$), were analyzed with Igor Pro software using customized scripts. V_{th} was defined as voltage at which dV/dt reached the level of 0.03 * (dV/dt_{max} – dV/dt_{min}) + dV/dt_{min} (Leipold et al., 2013). Trains of action potentials were evoked repetitively by 2-s current injections ranging from 0 to 180 pA in steps of 20 pA. Mean firing frequencies were determined using 0 mV as the action potential detection threshold.

Data analyses and statistics

We standardized individual QST parameters by comparison with healthy sex- and age-matched reference data from identical body regions. A normal distribution in log space was present in all QST parameters, except for thermal pain thresholds and the vibratory detection threshold. Dynamic mechanical allodynia and paradoxical heat sensations did not occur in the mother-and-son duo. Before statistical analyses, normally distributed values were logarithmically transformed. Z-score values were calculated from all these values using the term: $z = (mean_{patient} - mean_{controls})/SD_{controls}$, resulting in a standard normal distribution independent of age, sex, and body region. A z value > 0 indicates gain-of-function, corresponding to positive symptoms, and a z value < 0 indicates loss-of-function, corresponding to negative symptoms.

All electrophysiological recordings were analyzed using FitMaster (HEKA Elektronik) and Igor Pro (WaveMetrics) software. Corresponding data are presented as means ± SEM (n) with n being the number of independent experiments. Statistical analysis was carried out using GraphPad Prism version 8.0.1 software (GraphPad Software). Datasets were first tested for normality using the D'Agostino–Pearson test. Subsequently, statistical comparisons of two groups of data were made using two-sided Student's t test for normally distributed data or the Mann–Whitney rank sum test for non-normally distributed data. P values are reported together with the test used.

We conducted a comprehensive literature review focusing on the genotype-phenotype correlations, mode of inheritance, and functional evidence of published (likely) pathogenic *SCN11A* variants. Data sources included ClinVar, PubMed (PMID), and Online Mendelian Inheritance in Man (McKusick/Nathans Institute of Genetic Medicine, Johns Hopkins University, Baltimore, MD, USA, 2025). Search terms included *SCN11A*, "sodium voltage-gated channel alpha subunit 11," and "SFN." To evaluate the pathogenicity of identified variants, we applied the classification criteria established by the American College of Medical Genetics and Genomics.

Online supplemental material

Fig. S1 shows rectangular and half-sinusoidal axon stimulation. Fig. S2 shows sinusoidal axon stimulation. Table S1 shows (likely) pathogenic *SCN11A* variants and associated phenotypes.

Results

Both p.(Tyr66Ser) variant carriers present with SFN

Two patients (Fig. 1, A and B), a mother (patient I.1) and her son (patient II.2), presented to our outpatient clinic with sensory dysfunction, including episodes of ongoing neuropathic pain.

Patient I.1, index patient and mother of patient II.2 (Fig. 1 B), reported needle-like, pricking, and electric shock-like sensations, accompanied by burning pain in both feet, with initial manifestation 5 years prior to her first presentation. She was followed up in our outpatient clinic between the age of 58 and 63 years. During the first years of symptoms, prior to her initial consultation, the burning pain spread from toes to hips and from fingertips to shoulders (Fig. 1 AI and Table 1). The pain was quantified as 4/10 on the NRS (where 0 is no pain and 10 the worst imaginable pain). She was not taking analgesics. Using the PainDETECT questionnaire to detect neuropathic pain (Freynhagen et al., 2016), she scored 21/38 (Table 2), while no other pain-linked diseases were present. Thus, her clinical presentation is consistent with a neuropathic pain syndrome. In addition, she reported frequent burning sensations, paresthesias, a vibrating sensation in different body parts, and episodic sensations of cold in the whole body (Fig. 1 AII and Table 1). She suffered from numbness in feet and hypoesthesia for hot stimuli affecting the whole body, which were classified as negative symptoms (Fig. 1 AIII and Table 1). The only reported autonomic symptom was occasional dizziness (Table 1). The physical examination revealed the presence of cold thermal hypoesthesia in both feet, lower legs, and hands, and reduced perception of light touch at the right bodyside (Table 1). Muscle strength, deep tendon reflexes, and further sensory tests (vibration, position) were normal. Nerve conduction studies did not reveal any signs of large fiber involvement (Table 1). By skin biopsy, we quantified a reduced IENFD of 2.7/mm (Table 1). We diagnosed the patient with SFN.

The index patient's son, patient II.2 (Fig. 1 B), followed between the age of 32 and 37 years, reported similar symptoms with an onset at the age of 27 years. At the time of his first examination, he reported paresthesias (constant prickling) in both feet and hands, as well as numbness in feet that had progressed

Downloaded from rupress.org/jgp/article-pdf/157/6/e202413691/1952150/jgp_202413691.pdf by guest on 15 November 2026

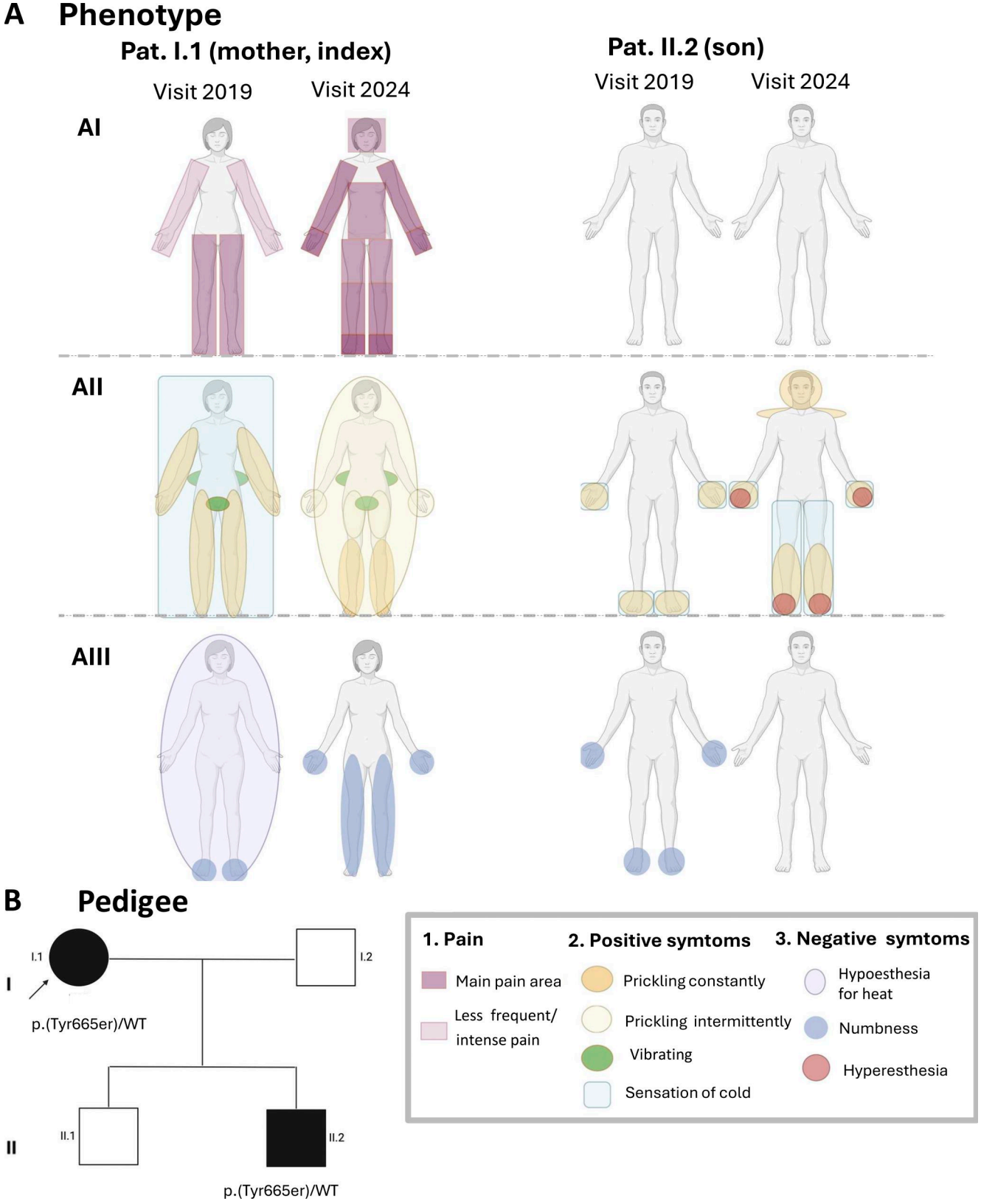


Figure 1. **Phenotype overview and pedigree. (A)** Clinical phenotypes: this schematic depicts clinically affected body regions, illustrating variable symptom clusters and their change over time. The darker the color, the stronger the pain. The parts of the body involved are colored. **(AI)** In rose, the regions affected by pain. **(AII)** In green, yellow and orange/red regions affected by other positive symptoms, colored by symptom (see also legends). **(AIII)** In blue, regions affected by negative symptoms. In patient I.1 (mother), pain levels intensified across the observation interval (AI), whereas sensory plus symptoms spread (AII) and minus symptoms changed with an increase in numbness and disappearing of hypoesthesia for temperature (AIII). Patient II.2 (son) had no neuropathic pain over

Downloaded from rupress.org/jgp/article-pdf/157/6/e202413691/1952150/jgp_202413691.pdf by guest on 15 November 2026

the years (AI). The positive sensory symptoms changed from hyperesthesia and consistent prickling to a sensation of cold and expansion of paresthesia (AII). Numbness disappeared (AIII) **(B)** Pedigree: the index patient (I.1) has two sons. The older son was reported to have no neuropathic pain, positive or negative sensory symptoms, but suffered from epilepsy of unknown etiology. The second son (II.2) and the index patient (I.1) were symptomatic (SFN), both carrying the p.(Tyr66Ser) variant in *SCN11A*. p.(Tyr66Ser)/WTWTA = heterozygous variant carrier.

to the hands (Fig. 1, AII and AIII; and Table 1). He further reported restless legs and a persistent cold feeling in hands and feet, even when extremities were warmed up (Fig. 1 AII and Table 1). There was no (neuropathic) pain, and he was not on any medication (Table 2). Like his mother, he only had mild autonomic symptoms, being limited to occasional constipation (Table 1). The patient had been treated for neuroblastoma at the age of 1 year (reportedly surgery and cytostatics); however, conclusive documents were not available (Table 1). In his initial clinical examination, he had no signs of large fiber neuropathy with normal muscle strength, tendon reflexes, and vibration perception. Accordingly, nerve conduction studies were unremarkable. Instead, we found a reduced perception of touch and cold in his left arm and both feet, together with decreased pinprick discrimination in his right foot and thermal hypoesthesia in his fingers and feet. His skin biopsy, obtained at the age of 32 years from his distal lateral lower leg, was normal with an IENFD of 8.7/mm (Table 1). By QST, we found significant dysfunction of Aδ- and C-nerve fibers (see below).

Neither disease histories nor blood parameters revealed any other acquired cause of SFN in patients I.1 and II.2. There was no indication of autoimmune disorder, no vitamin deficiency, and no exposure to significant neurotoxins in the recent past. Upon family history (Fig. 1 B), no further affected individuals were reported. The index patient's oldest son suffered from epilepsy of unknown cause with generalized seizures.

Symptoms intensify in both patients during longitudinal follow-up

Both patients carried the potentially disease-causing variant since birth, but disease onset occurred during adulthood, and symptoms progressively worsened, albeit with fluctuations. Patient I.1 underwent three clinical follow-up evaluations: the first 26 mo (2021), the second 56 mo (2023), and the final examination 66 mo (2024) after her initial presentation at our clinic. Patient II.2 was re-examined 26 and 66 mo after baseline.

At 26 and 56 mo, patient I.1 reported the highest pain intensity in her lower extremities, whereas involvement of the upper extremities was episodic. By the time of the last follow-up, the areas affected by pain had expanded to the trunk and face (Fig. 1 AI, Table 2). The pain intensity increased gradually over time, with an NRS rise from 2 to 7 at the lower extremities and from 1 to 6 at the upper extremities (Table 2). She was started on capsaicin cream for local pain management, and at the time of her last follow-up visit, she had begun to use transcutaneous electrical nerve stimulation (TENS) (Table 2). An almost permanent sensation of cold that significantly contributed to the phenotype in the first years of disease disappeared during follow-up. Instead, the patient developed pruritus as a new positive symptom, localized to the palms of her hands, which occurred in 2023 and expanded to the upper legs in 2024 (Table 2). Paresthesia spread intermittently across the body surface, but constant paresthesias in the extremities disappeared in the patient's arms (Fig. 1 AII). Patient II.2, milder affected overall, did not report any ongoing pain, but rather constant prickling (paresthesia) that by month 66 had expanded from the extremities to the neck, face, and scalp (Fig. 1 AII). He described disease progression to be gradual with episodic sensory symptoms, especially cold sensations in hands, feet, and legs and hypersensitivity to heat in the distal extremities (Fig. 1 AII). Subjectively, symptoms became more intense with lower ambient temperatures, e.g., during colder seasons.

In both patients, a notable degree of variability was observed for negative sensory signs. In patient I.1, numbness was initially observed in the feet, disappeared, and returned in an expanded form, in contrast to general hypoesthesia that remained constant until the most recent follow-up (Fig. 1 AIII). As a new negative symptom, patient I.1 reported reduced sensitivity to heat that was noted throughout the entire body, during the 26-mo follow-up. All negative symptoms reported by patient II.2 in 2019 had disappeared in 2024 (Fig. 1 AIII).

Whereas in patient I.1, the physical examination remained largely unchanged, except for fluctuations in light touch perception, throughout the follow-ups, clinical sensory testing in patient II.2 revealed that affected areas of reduced cold and pinprick perception spread along both arms and legs, and the perception of light touch recovered over time (Table 2).

Assessing autonomic symptoms at baseline, patient I.1 reported occasional dizziness only, with one episode of unconsciousness mentioned at the subsequent visit. Schellong's test for orthostatic blood pressure regulation was normal at the first visits, turned borderline pathological (10 mmHg reduction in diastolic blood pressure) in 2023, and returned to normal in 2024. Patient II.2's autonomic symptoms were limited to mild constipation initially; however, sicca symptoms (dryness of mouth and eyes) developed across the observation interval in both individuals. Similarly, in patients I.1 and II.2, the electrochemical skin conductance decreased moderately over time, indicating disturbed C-fiber–mediated sweat gland innervation upon Sudoscan testing.

Both patients display typical thermal hypoesthesia on QST

Patient I.1 underwent four consecutive QST investigations between 2019 and 2023 (Fig. 2 A and Table 2) on the right foot dorsum (most affected test area) and the back of her right hand (least affected area). Interestingly, we found a very similar pattern in both areas: there were significant thermal hypoesthesia with reduced cold detection thresholds (CDTs), increased warmth detection thresholds (WDTs, meaning reduced warmth detection), and increased thermal sensory limina (TSL) (Fig. 2 A). From 2019 to 2023, the increased WDT spread from the back of the hand to the foot. We observed mild heat pain hypoalgesia

Downloaded from rupress.org/jgp/article-pdf/157/6/e202413691/1952150/jgp_202413691.pdf by guest on 15 November 2026

Table 1. **Symptoms, clinical, and paraclinical examinations of mother and son at baseline**

	Mother (I.1)	Son (II.2)
Symptoms		
Duration (years)	5	5
Neuropathic pain	yes	no
Sensory		
Negative	numbness (f), hypoesthesia (tb)	numbness (f, h)
Positive[a]	paresthesia (e), cold sensation (tb), vibration feeling (p)	paresthesia (f, h), cold sensation (f, h)
Autonomic	dizziness	constipation
Other	-	restless legs
Medical history	-	neuroblastoma
Clinical examination		
Sensory		
Light touch	↓ bodyside (r)	↓ a (l), f
Temperature	↓ f, h,leg	↓ fing, f
Pinprick perception	normal	↓ f (r)
Large fiber		
Tendon reflexes	normal	normal
Vibration perception	normal	normal
Muscle weakness	no	no
Gait	normal	normal
Paraclinical examinations		
Nerve conduction studies	normal	normal
Sweat test (Sudoscan)	normal	normal
QST	Aδ-, Aβ-, and C-fiber dysfunction	Aδ- and C-fiber dysfunction
Skin biopsy (IENFD)	reduced (2.7/mm)	normal (8.7/mm)
Schellong's test	normal	normal
Laboratory work	normal	normal

a, arm; e, extremities; f, feet; fing, fingers; h, hands; leg, legs; p, pelvic and pubic region; tb, total body; r, right; l, left; ↓, reduced.
[a]Positive symptoms other than neuropathic pain.

(heat pain threshold [HPT]) throughout the years (Fig. 2 A). As signs of gain-of-fiber-function, we observed pinprick hyperalgesia at the foot dorsum only. In both areas, we detected increased mechanical pain sensitivity (allodynia), which can be interpreted as a sign of central sensitization. At the first, but not the most recent visit, the mechanical detection threshold was reduced, suggesting potential Aβ-fiber dysfunction (Fig. 3).

Interestingly, the sensory profile of the son, patient II.2, although less explicit, was quite similarly characterized by thermal hypoesthesia (Fig. 2 A). Patient II.2 underwent four QST investigations between 2019 and 2024 on the back of the left foot and the right hand as test areas, both equally affected. CDT was reduced in 2019 and 2024, whereas TSL was increased in 2024 (Fig. 2 A). Heat pain hypoalgesia did not change significantly; however, there was a declining trend in CPT and HPT values (loss-of-fiber-function for each) in 2024. We found pinprick hyperalgesia throughout the last two follow-up examinations.

Summarizing both patients' results, sensory negative signs (thermal hypoesthesia in mother and son and heat pain hypoalgesia in the mother) all pointed toward loss-of-fiber-function, whereas pinprick hyperalgesia suggested gain-of-fiber-function.

PREPs are consistent with small fiber dysfunction

To assess the central pain pathway in both patients, we used PREPs. In contrast to patient I.1 (mother), patient II.2 (son) exhibited slightly reduced PREP amplitudes upon nociceptive, electrical stimulation of his dorsal hand (Fig. 2 B), consistent with potential Aδ-fiber dysfunction. In both examined patients, we did not find reproducible PREP responses to stimulation at the feet, pointing toward a more significant fiber loss or a length-dependent loss-of-fiber-function.

Electrical psychophysics indicate activation of CMi-fibers (sleeping nociceptors)

Abnormal pain responses to rectangular stimulation were interpreted as dysfunction of A-fibers, whereas pathological responses to half-sine-wave stimulation pointed toward dysfunction of C-fibers responsive to mechanical stimuli (CM-fibers), and sine-wave stimulation was used to conclude on mechanically insensitive (CMi-) fibers.

Upon rectangular electrical suprathreshold stimulation, patient I.1 showed a similar stimulus-response curve in pain ratings as controls: no pain at low amperage 0.25–1 mA, but relatively high pain ratings (10–15 on the NRS) at 2 mA and above (second to third quartiles) (Fig. S1 A). Patient II.2 had similar arm responses, while pain ratings substantially exceeded the control maximum from 2 mA onward at the foot dorsum (15–45 on the NRS) (Fig. S1 A). Looking at frequency–response curves, we observed slightly increasing pain ratings from 4 to 100 Hz in controls, whereas patient I.1 consistently reported high pain ratings. Interestingly, there was a sudden substantial increase in pain ratings for patient I.1 during stimulation change from 4.6 to 10 Hz to higher frequencies of 20, 50, and 100 Hz (at the arm from NRS 20–40 to NRS 70 and at the foot from NRS 10–15 to NRS 40–70). (Fig. S1 B). Patient II.2's ratings were in the range of healthy controls (50th–75th percentile, 20–15 on the NRS) at the arm, but decreased over time to lower percentiles (10th–25th percentile), while the controls' ratings, in contrast, increased (median 9.5–30) (Fig. S1 B). At the foot, patient II.2 rated pain with a similar frequency dependency as controls, but in much higher intensities, twice exceeding the 90th percentile (Fig. S1 B). Upon half-sine-wave stimulation, both patients showed a similar stimulus–response curve as controls, except for the

Downloaded from rupress.org/jgp/article-pdf/157/6/e202413691/1952150/jgp_202413691.pdf by guest on 15 November 2026

Table 2. **Neuropathic pain and follow-up data**

	Mother (I.1)				Son (II.2)		
Follow-up (months)	0	26	56	66	0	26	66
Neuropathic pain	P	P	P	P	-	-	-
PainDETECT (X/38)	21	13	10	15	-	-	-
NRS score (X/10)							
Lower extremities	MD	2	4	7	0	0	0
Upper extremities	MD	1	3	6	0	0	0
Trunk and face	MD	0	0	4 & 3	0	0	0
Itch	-	-	P	P	-	-	-
Allodynia	-	-	-	-	-	-	-
Pain medication			Caps	Caps & TENS			
Clinical examination							
Light touch	↓	N	↓	N	↓	N	N
Temperature	↓	N	↓	↓	↓	↓	↓
Pinprick perception	N	N	↓	N	↓	↓	N
Paraclinical examinations							
Nerve conduction studies	N	N	MD	N	N	N	N
Sweat test (Sudoscan)	N	N	P	P	N	N	P
QST	P	P	P	P	P	N	P
Schellong's test	N	MD	P	N	N	N	N

Caps, topical capsaicin treatment; TENS, transcutaneous electrical nerve stimulation; -, absent; N, normal; MD, missing data; P, pathological/present; ↓, reduced; QST, quantitative sensory testing.

highest stimulation intensity, where both patients reported increased pain ratings (Fig. S1 C).

In controls, electric sinusoidal skin stimulation that is supposed to activate CMi-fibers (Jonas et al., 2018) induced mild pain, which increased with higher stimulation intensities. At low amperage (0.025–0.1 mA), patient I.1 reported no pain. With higher stimulation amperages (0.2, 0.3, and 0.4 mA), however, she rated pain intensities above the controls' maximum at both hand and foot (Fig. 2 C.a, b; and Fig. S2 A). Patient II.2 presented with a similar pattern. With stepwise increasing stimulation frequencies, healthy controls showed relatively, particularly at the foot, stable pain ratings around NRS 20 (out of 100). At low frequencies, patient I.1 reported similar pain ratings, which, however, dropped for higher frequencies. At the arm level, 100 Hz was not perceived as painful (pain rating 0), indicating that C-fibers were not able to follow higher stimulation frequencies (Fig. S2 B). Similarly, foot pain ratings dropped from above control level for low stimulation frequencies (4 Hz) to pain ratings within normal range at higher stimulation frequencies (100 Hz) (Fig. S2 B). When continuously stimulated over a period of 1 min, healthy controls showed the expected range of adaptation (Jonas et al., 2018), whereas both patients reported consistently higher pain ratings (patient I.1 within 90th percentile, patient II.2 over the 90th percentile at the arm level). While patient I.1 did not show any adaptation in pain ratings, patient II.2's ratings decreased slightly at arm, but not at foot level. At the foot level, data from patient I.1 were not interpretable (Fig. S2 C). At the applied amperage of ∼0.4 mA, sinusoidal electrical pulses activate CMi-fibers, which comes with widespread axon reflex erythema. Patient II.2 showed an axon flare within the upper control range at both the arm and foot (75th–90th percentile). At the foot, the size of detectable erythema exceeded the control maximum within the first 10 s of stimulation (0–10 s). In contrast, patient I.1 exhibited a relatively small erythema at the arm, most of the time under the 10th percentile, whereas data from her foot were of too low quality for interpretation (Fig. S2 D).

Co-segregating *SCN11A* variant p.(Tyr66Ser) is a candidate to explain the phenotype

By whole-exome sequencing, we identified the heterozygous variant NM_001349253.2:c.197A>C; p.(Tyr66Ser), Chr3: g.38950166T>G (hg38) in the $Na_V1.9$-encoding gene, *SCN11A*, in both mother and son, cosegregating with the SFN phenotype (described above). No additional pathogenic or likely pathogenic variants were detected in this or other genes associated with sensory disorders that might otherwise explain the patients' phenotype. To date, the variant is not present in control databases (gnomAD v4.1.0, ExAC), neither has it been associated with any disease phenotype prior to this study. Located in exon 5 (of 30), it affects the N-terminal part of $Na_V1.9$ slightly upstream of the first transmembrane domain (D1S1), (Fig. 3, A, C, and D), without other reported pathogenic variants in close vicinity. At the same amino acid position, however, two individuals from the

Downloaded from rupress.org/jgp/article-pdf/157/6/e202413691/1952150/jgp_202413691.pdf by guest on 15 November 2026

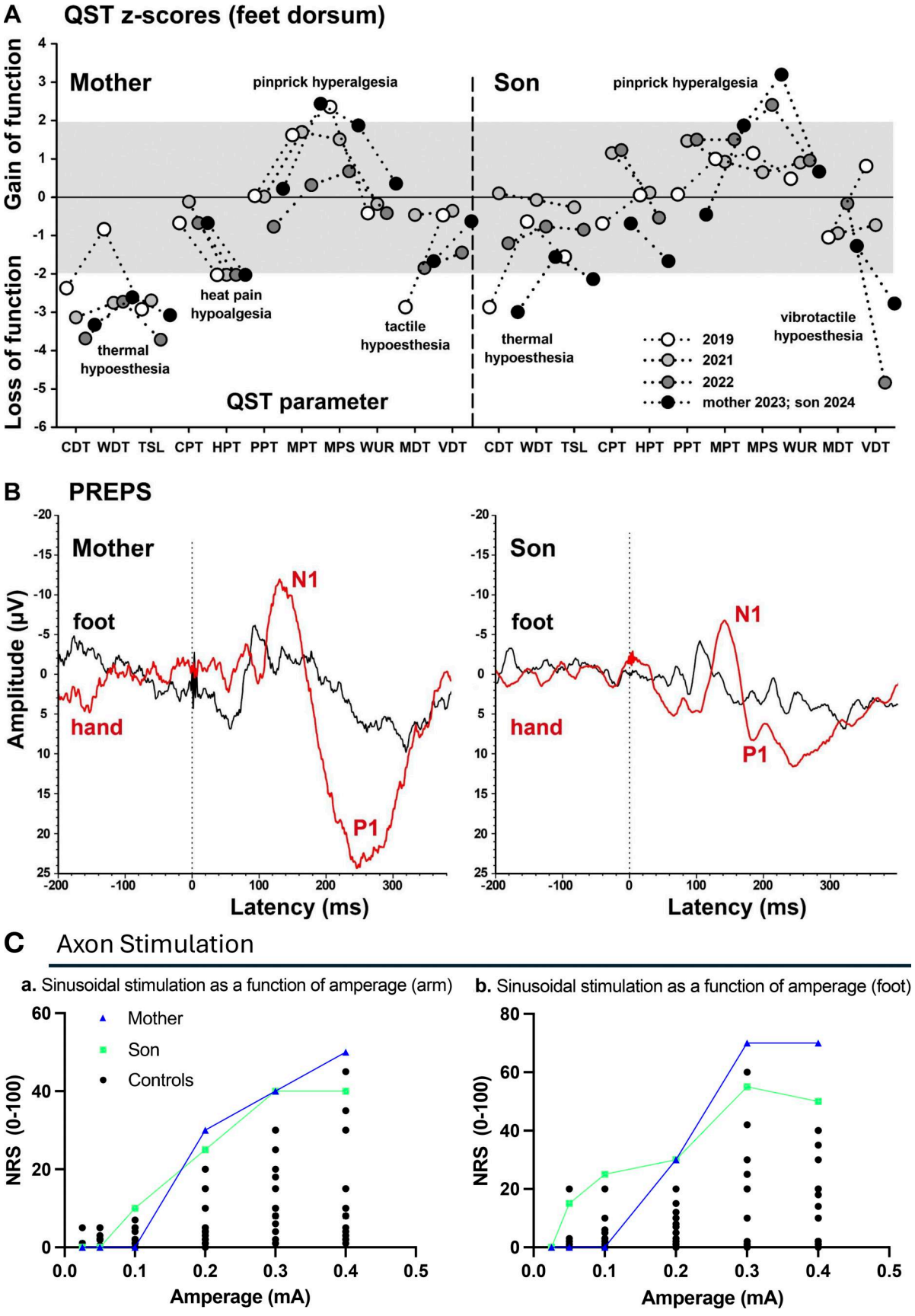


Figure 2. **QST, pain-evoked potentials, and axon stimulation. (A)** The QST z-scores for the foot dorsum indicate a similar sensory profile in both mother (I.1) and son (II.2), characterized by thermal hypoesthesia, which serves as a clinical marker of impaired function in small nerve fibers (Aδ- and C-fibers). In the

Downloaded from rupress.org/jgp/article-pdf/157/6/e202413691/1952150/jgp_202413691.pdf by guest on 15 November 2026

mother, this is accompanied by heat hypoalgesia. In a few measurements of mother and son, there is also a (vibro-)tactile deficit, suggesting compromised function of large fibers (Aβ-fibers). These negative sensory signs are associated with the positive sign of mechanical hyperalgesia to pinprick stimuli, which is consistent with the concept of secondary central sensitization in the nociceptive system. **(B)** PREPs objectively demonstrate the performance of Aδ-fiber–mediated nociceptive responses following electrical stimulation of the skin on the hand and foot dorsum. A normal potential is only recordable in the mother after hand stimulation. In patient II.2, PREPs show a reduced amplitude, which is consistent with an axonal functional or structural deficit affecting these fibers. The responses following foot stimulation are not clearly distinguishable in both subjects. **(C)** Pain intensity ratings on the NRS 0–100 during sinusoidal axon stimulation for the mother, son, and 20 controls. Sine-wave stimulation as a function of amperage at 4 Hz on the dorsum of the arm (C.a) and foot dorsum (C.b): electric sinusoidal skin stimulation induced mild pain in controls, increasing with higher stimulation intensities. At low amperage, both patients did not report any pain. With higher stimulation amperages (0.2, 0.3, and 0.4 mA), however, they rated pain intensities above the controls' maximum at both hand and foot (Fig. 3 C.a, b), showing a similar pattern.

GnomAD v4.1.0 database without any reported disease phenotype carry the variant p.(Tyr66Cys) that has to be considered a variant of unknown significance. The affected tyrosine residue is conserved through species (GERP 5.41) and across all nine human Na_Vs (Fig. 3 B). As rated by *in silico* prediction tools, the p.(Tyr66Ser) variant is potentially pathogenic (CADD 14.8, Phred score: 24.6).

The variant p.(Tyr66Ser) affects activation and fast inactivation of $Na_V1.9$

To assess the impact of the p.(Tyr66Ser) variant on channel function, whole-cell voltage-clamp recordings were performed in $Na_V1.8/Na_V1.9$ DKO DRG neurons transfected with expression plasmids encoding either wild type $Na_V1.9$ or $Na_V1.9$-Tyr66Ser channels. All measurements were carried out in the presence of TTX (1 μM) to inhibit Na^+ currents endogenous in $Na_V1.8/Na_V1.9$ DKO DRG neurons and to isolate specifically the TTX-resistant $Na_V1.9$-dependent currents (Loose et al., 2023). As shown in Fig. 4 A, both wild type and $Na_V1.9$-Tyr66Ser channels gave rise to robust Na^+, currents characterized by slow activation and inactivation kinetics typical for $Na_V1.9$. Compared with the wild type, the $Na_V1.9$-Tyr66Ser variant displayed reduced inward current densities, specifically at low membrane voltages. Analysis of the voltage dependence of peak current densities (Fig. 4 B) and the voltage dependence of activation and deactivation kinetics (Fig. 4 C) revealed that $Na_V1.9$-Tyr66Ser channels activated more slowly and deactivated more quickly (Fig. 4 D) than $Na_V1.9$ wild type compatible with a rightshift of the voltage of half-maximal channel activation, V_m, by 16.6 mV ($Na_V1.9$: −61.9 ± 1.4 mV, p.(Tyr66Ser): −45.3 ± 3.2 mV, $P < 0.001$, two-sided *t* test). The corresponding slope factor (*km*), reflecting the voltage dependence of channel activation, was slightly yet significantly increased in $Na_V1.9$-Tyr66Ser ($Na_V1.9$: 6.0 ± 0.4 mV, p.(Tyr66Ser): 7.6 ± 0.4 mV, $P < 0.01$, two-sided *t* test). The voltage dependence of activation and deactivation kinetics (Fig. 4, C and D) yielded a gating charge transfer of 2.3 ± 0.2 e_0 and 2.4 ± 0.1 e_0 and symmetry factors specifying the charge fraction assigned to channel activation of 0.47 ± 0.14 and 0.48 ± 0.10 for wild type and $Na_V1.9$-Tyr66Ser, respectively.

Similar to channel activation, the voltage dependence of steady-state channel inactivation was also affected by p.(Tyr66Ser). The p.(Tyr66Ser) alteration shifted the voltage of half-maximal steady-state channel inactivation, V_h, to significantly higher values ($Na_V1.9$: −72.1 ± 1.6 mV, p.(Tyr66Ser): −58.2 ± 3.3 mV, $P < 0.01$, two-sided *t* test), effectively increasing functional channel availability (Fig. 4 E). However, the corresponding slope factor was not affected by p.(Tyr66Ser) ($Na_V1.9$: 9.5 ± 0.4 mV, p.(Tyr66Ser): 9.4 ± 0.5 mV, $P > 0.05$, two-sided *t* test). In addition, kinetics of fast channel inactivation were slowed down in $Na_V1.9$-Tyr66Ser channels (Fig. 4, A and F). Thus, the p.(Tyr66Ser) alteration confers loss-of-function and gain-of-function attributes to $Na_V1.9$ by affecting both channel activation and inactivation.

The effects of the p.(Tyr66Ser) variant on neuronal excitability were examined in current-clamp recordings obtained from small-diameter (<25 μm) DRG neurons isolated from wild type mice and subsequently transfected with cDNA constructs encoding either human $Na_V1.9$ or $Na_V1.9$-Tyr66Ser. While neurons transfected with the p.(Tyr66Ser) variant mimicked the heterozygous situation present in the patients, neurons transfected with the wild type construct were used as controls. As shown in Fig. 4, G and H, the overexpression of $Na_V1.9$-Tyr66Ser shortened the width ($Width_0$, $Na_V1.9$: 4.0 ± 0.3 ms, p.(Tyr66Ser): 3.1 ± 0.2 ms, $P < 0.05$, two-sided *t* test) and decreased the minimum V_{AHP} ($Na_V1.9$: −78.0 ± 1.0 mV, p.(Tyr66Ser): −81.4 ± 1.1 mV, $P < 0.05$, two-sided *t* test) of individual action potential waveforms. Other parameters characterizing the action potential waveforms, such as the resting membrane potential, the threshold voltage for action potential firing (V_{th}), and the action potential peak voltage (V_{peak}), were not affected by the overexpression of $Na_V1.9$-Tyr66Ser channels (all $P > 0.05$, two-sided *t* test). Firing rates of transfected neurons were determined by evoking repetitive action potentials with 2-s current injections ranging from 0 to 180 pA in steps of 20 pA. Although neurons overexpressing the p.(Tyr66Ser) variant tended to generate fewer action potentials in response to low (<100 pA) stimulation intensities and more in response to high stimulation intensities when compared to neurons overexpressing $Na_V1.9$ wild type, the mean firing rates were not significantly different between the two groups (Fig. 4, I and J).

Discussion

In this study, we identified the novel heterozygous *SCN11A* missense variant p.(Tyr66Ser), which segregates in two family members with small fiber dysfunction and affects the activity of voltage-gated $Na_V1.9$ channels. Prospectively monitoring disease progression over several years, our observations yielded a detailed dataset covering multiple aspects of sensory function. As a primary symptom, both patients reported spontaneous cold sensations that partially recovered in patient I.1, who then developed pruritus and intermittent paresthesias, whereas patient

Downloaded from rupress.org/jgp/article-pdf/157/6/e202413691/1952150/jgp_202413691.pdf by guest on 15 November 2026

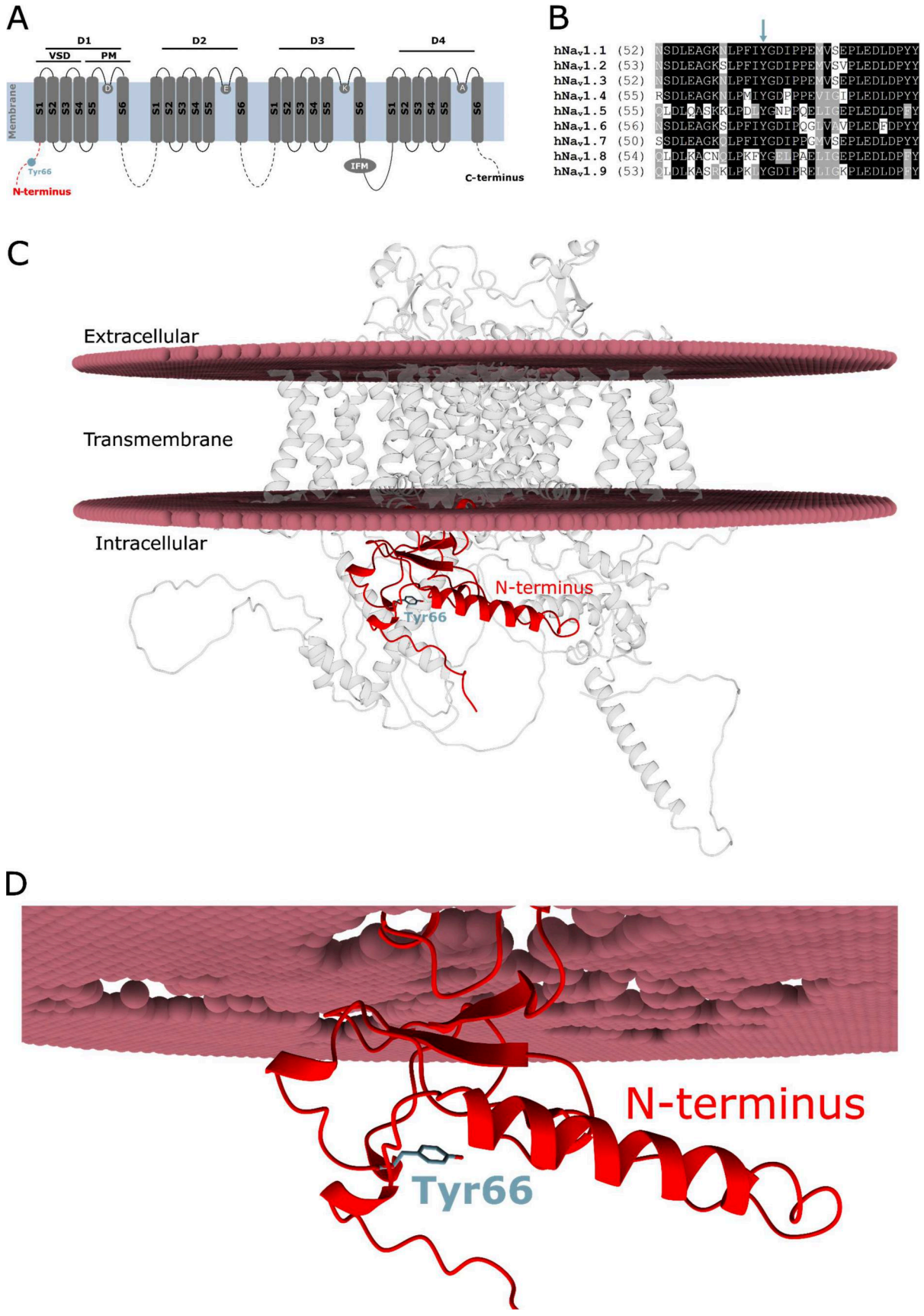


Figure 3. **Structural location and sequence conservation of hNa$_V$1.9 Tyr66Ser. (A)** Membrane topology of a Na$_V$. Na$_V$s are transmembrane proteins that consist of four homologous domains (D1–D4), each composed of 6 transmembrane helices (S1–S6). For each domain, S1–S4 make up the voltage sensor (VSD),

Downloaded from rupress.org/jgp/article-pdf/157/6/e202413691/1952150/jgp_202413691.pdf by guest on 15 November 2026

while S5–S6 form the PM that selects for sodium via the selectivity filter ("DEKA" motif). After opening, Na_Vs are quickly inactivated via the fast inactivation "IFM" motif. Position of p.(Tyr66Ser) in the channel N terminus is highlighted. **(B)** Multiple sequence alignment of all nine human Na_V subtypes ($Na_V1.1$–$Na_V1.9$). The letters represent the one-letter codes for each amino acid, and the starting numbers of each sequence are given inside parentheses. Only the N-terminal region around Tyr66Ser is shown for clarity. Dark boxes show fully conserved residues, gray boxes show partially conserved residues, and nonshaded boxes show nonconserved residues. Tyr66 is fully conserved across all nine subtypes (marked with an arrow). **(C)** 3D spatial location of Tyr66. The $hNa_V1.9$ model predicted by AlphaFold (AF-Q9UI33-F1) was downloaded and aligned to a bilayer membrane via the PPM server. The N terminus is highlighted in red for clarity. Tyr66 is located intracellularly in the N-terminal region. **(D)** Close-up of the Tyr66 residue. Tyr66 seems to be exposed intracellularly and might be involved in phosphorylation. PM, pore module.

II.2 continued to experience symptom aggravation at colder ambient temperatures. Upon QST, thermal hypoesthesia was a dominant pattern in both individuals over time, consistent with both C- and Aδ-fiber loss-of-function. Reduced PREP amplitudes supported that finding in patient II.2, and IENFD was reduced as a significant sign of small fiber degeneration in patient I.1. Axon stimulation revealed, similarly for both individuals, overshooting pain responses upon rectangular and sine-wave stimulation, supporting a pattern of Aδ- and C-fiber gain-of-function, with CMi-fibers being overly active and less adaptive. Interestingly, patch-clamp studies reflected these mixed gain- and loss-of-function properties at the channel level. As demonstrated by voltage-clamp recordings, the p.(Tyr66Ser) alteration resulted in robust depolarizing shifts of both $Na_V1.9$ activation and inactivation.

When presenting in the clinics, one patient (I.1) had neuropathic pain, the other patient (II.2) did not, but both carried the same *SCN11A* missense variant. This observation, together with the changes in clinical patterns over time, illustrates how tenuous the link between genotype and phenotype can be. It remains challenging to interpret the role of additional genetic and environmental factors contributing to or potentially even mitigating disease severity. Phenotype heterogeneity, as has been observed for *SCN11A* variants before (Zhang et al., 2013; Huang et al., 2014; Okuda et al., 2016; Han et al., 2017; Leipold et al., 2015), is indeed an important point when evaluating a variant's pathogenicity (Table S1).

Despite both patients meeting the international criteria for SFN (Devigili et al., 2008), we noticed some variability in their onset age and early symptoms: patient I.1 (mother) developed first symptoms at the beginning of her sixth decade, whereas patient II.2 (son) reported initial symptoms at 27 years old. While neuropathic pain remained the leading symptom in patient I.1 over time, patient II.2 did not report any pain. Common features in both individuals were spontaneous cold sensations, some degree of variable negative symptoms, and the development of mild autonomic signs (sicca symptoms and reduced sudomotor function) over time. For interpretation, abnormal cold perception might be of particular relevance here, given that $Na_V1.9$ has previously been shown to play an important role in cold detection (Nagao et al., 2025; Lolignier et al., 2015; Leipold et al., 2015; Matsubara et al., 2021). Therefore, altered biophysics due to the p.(Tyr66Ser) variant may have a direct impact on how cold fibers respond to stimulation. Over the observation interval of 5 years, we noticed mild progression of symptom intensity and distribution in both patients. Semi-objective measurements of sensation thresholds (QST) and stimulated pain perception (axon stimulation) revealed similar patterns, again, all pointing toward a mixed pattern of loss- and gain-of-fiber-function, with increased activity and decreased adaptation of CMi-fibers as a common feature. Due to the relevant age gap between the two patients at examination, it is conceivable that the clinical patterns and courses might further approximate or display new differences in the future. Specifically, sine-wave electrical stimulation revealed the same obvious aberrant stimulus–response curve in both individuals: pain responses remained similar to controls at low, but peaked with high, stimulation intensities. Relatedly, the firing frequencies of neurons overexpressing the variant tended to be reduced at low stimulation intensities and increased at high stimulation intensities. Overshooting responses, observed upon sine-wave stimulation in patient I.1, occurred in an on/off-like pattern. Since low-intensity half-sine-wave stimulation between 0.1 and 1 mA specifically targets mechanosensitive C-fibers (CM) and sine-wave stimulation activates both mechanosensitive CM and mechanoinsensitive CMi-fibers (Weidner, 1999; Jonas et al., 2018; Rukwied et al., 2020), we conclude that sensory responses can be at least partially attributed to the activity of CMi-fibers. Another interesting observation was the lack of adaptation during one-min sine-wave stimulation, which occurred in controls like reported in the literature (Jonas et al., 2018), but not in our patients. Especially in patient I.1, these results point toward axonal hyperexcitability with a particular involvement of CMi-fibers as a correlate of neuropathic pain. Apparently as a mismatch with that, the same patient (I.1) only developed a small-sized axon flare, which seems surprising, since the size of the axon reflex erythema has been hypothesized to correlate with CMi-fiber activation (Bickel et al., 2002). This discrepancy might at least partially be explained by the reduced IENFD observed in patient I.1. Although CMi-fibers usually terminate below the basal membrane and are therefore underrepresented in skin biopsies, it appears reasonable that this fiber class is affected by degeneration as well. Rarefication of the terminal tree of CMi-fibers might lead to insufficient calcitonin gene–related peptide release to reach the necessary dose for vasodilation; however, the remaining branches might be enough to induce pain during high-amplitude sinusoidal stimulation. Additionally, CMi-fibers whose endings might be degenerated could still be present in deeper skin layers and produce spontaneous activity. Patient II.2's IENFD, in comparison, was within normal limits, and his axon flare was in the upper percentiles of controls. Whether this is mainly explained by CMi-fiber hyperexcitability or merely because of increased efferent function or hyperfunction of skin blood vessels remains unclear. Of note, patient II.2 was younger (35 years) and patient I.1 older (58 years) than the control median age (48 years) at the time of investigation. Consequently,

Downloaded from rupress.org/jgp/article-pdf/157/6/e202413691/1952150/jgp_202413691.pdf by guest on 15 November 2026

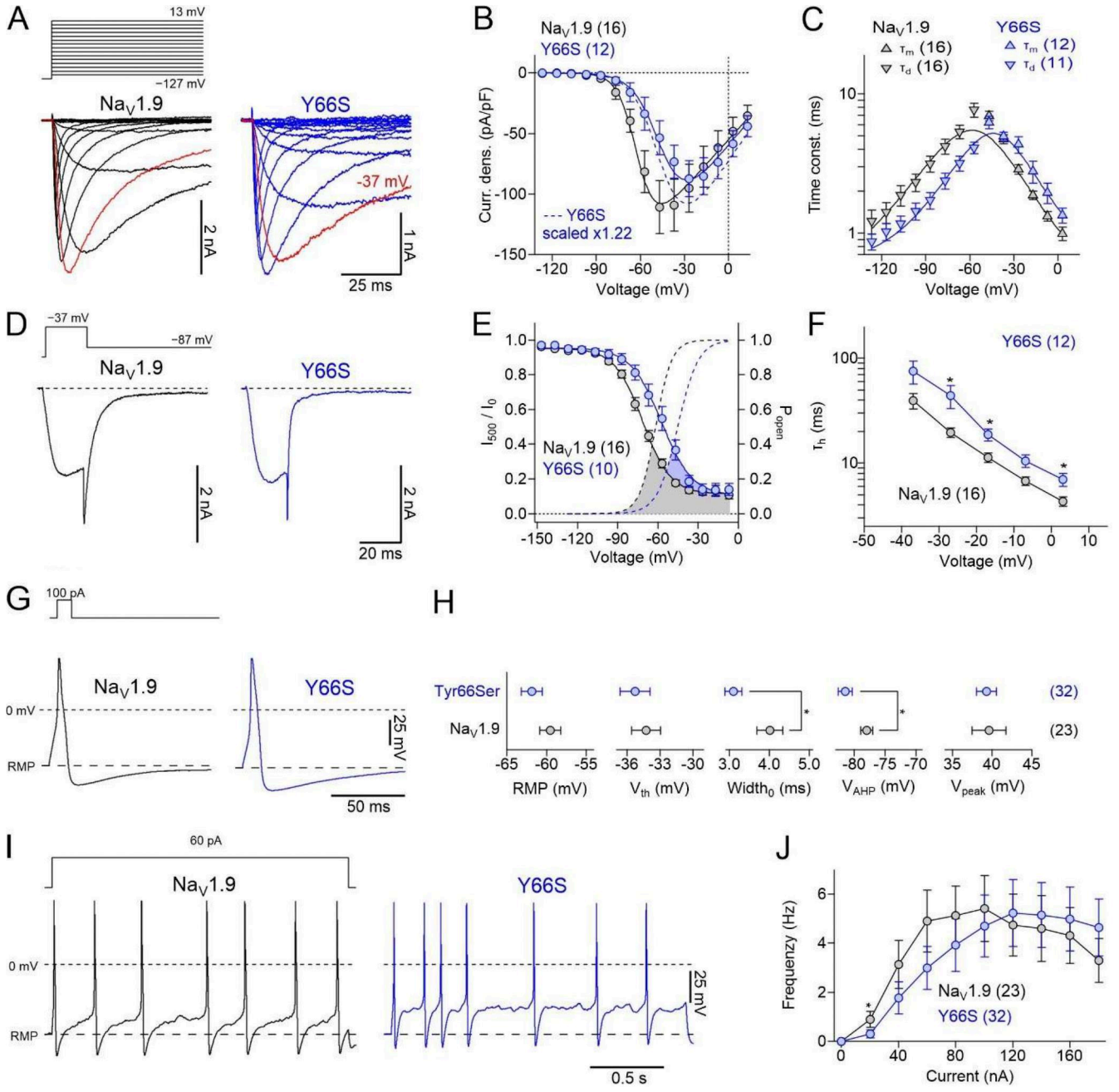


Figure 4. **The variant p.(Tyr66Ser) effects on activation and inactivation properties of Na$_V$1.9 channels. (A)** Representative whole-cell current traces recorded from Na$_V$1.8/Na$_V$1.9 DKO DRG neurons, expressing human Na$_V$1.9 (black) or Na$_V$1.9-Tyr66Ser (alternative nomenclature: Y66S), (blue) channels, in response to depolarizations ranging from −127 to 13 mV in steps of 10 mV. Current responses obtained at a voltage of −37 mV are highlighted in red. The corresponding pulse protocol is shown on top. **(B)** Mean peak current densities obtained from experiments as shown in A, plotted as a function of voltage. Solid curves are data fits according to Eq. 1 describing the voltage dependence of channel activation. The dashed line is the data fit to Na$_V$1.9-Tyr66Ser, scaled in magnitude by a factor of 1.22. **(C)** Time constants of channel activation (τ_m) and channel deactivation (τ_d) obtained from current traces as shown in A and D, respectively, plotted as a function of voltage. Superimposed curves are data fits according to Eq. 3 characterizing the voltage dependence of activation and deactivation kinetics. **(D)** Representative whole-cell tail currents of Na$_V$1.9 wild type and Tyr66Ser mutant channels in response to a hyperpolarizing voltage step from −37 to −87 mV (top) to characterize channel deactivation. **(E)** Voltage dependence of steady-state fast inactivation of Na$_V$1.9 (black) and Na$_V$1.9-Tyr66Ser (blue) channels with superimposed fits (solid curves) according to Eq. 2. Dashed curves are the voltage-dependent open probabilities of Na$_V$1.9 and Na$_V$1.9-Tyr66Ser, estimated from data fits as shown in B according to Eq. 1. **(F)** Single-exponential time constants characterizing inactivation kinetics of Na$_V$1.9 and Tyr66Ser mutant channels, plotted as a function of voltage. Straight lines connect data points. **(G)** Representative evoked action potentials of DRG neurons transfected with plasmids encoding either Na$_V$1.9 (black) or Na$_V$1.9-Tyr66Ser (blue), in response to 10-ms current injections of 100 pA (top). Dotted lines mark 0 mV; dashed lines indicate the level of the RMP. **(H)** Parameters characterizing action potential properties. RMP: resting membrane potential; V_{th}: action potential threshold voltage; $Width_0$: action potential duration at 0 mV; V_{AHP}: maximal after-hyperpolarization voltage; V_{peak}: action potential peak voltage. **(I)** Representative trains of action potentials recorded in DRG neurons transfected with wild type Na$_V$1.9 (black) or mutant Tyr66Ser (blue), in response to 2-s current injections of 60 pA. Dotted lines mark 0 mV; dashed lines indicate the level of the RMP. **(J)** Action potential frequencies as a function of injected current obtained from experiments as shown in I. Data points in B, C, E, F, H, and J are means ± SEM with the numbers of neurons analyzed, *n*, indicated in parentheses. Asterisks refer to a Mann–Whitney rank sum test (F and J) or to two-sided Student's *t* test: *P < 0.05. RMP, resting membrane potential.

Downloaded from rupress.org/jgp/article-pdf/157/6/e202413691/1952150/jgp_202413691.pdf by guest on 15 November 2026

patient I.1 may have hyperexcitable, but fewer, CMi-fibers overall, which could account for her reduced neurogenic vasodilation. Overall, patient II.2 reported higher pain ratings primarily during one-min and frequency-dependent sinusoidal stimulation. In alignment with clinical and QST findings, he rated pain levels higher at the foot dorsum compared with stimulation at the arm level. Normal PREP amplitudes in patient I.1 and only slightly reduced amplitudes in patient II.2 following stimulation of the hand, alongside the poorly defined potentials upon foot stimulation, are consistent with the concept of a length-dependent structural or functional deficit of nociceptive Aδ-fibers. Given that patient I.1 has experienced daily neuropathic pain for years, central sensitization mechanisms as validated by QST could plausibly contribute to the observed differences in the clinical phenotype, including pain ratings as a response to stimulation and the according lack of adaptation. Taken together, we observed a sudden, overshooting leap in pain ratings upon sinusoidal electrical stimulation, which we called an on/off phenomenon, as a potentially Na_V variant–specific phenotypical feature, which is uniformly present in both patients. The differences in clinical phenotype between the two patients and other more subtle alterations in electrical psychophysics might be influenced and shaped by cofactors on different levels such as age, nerve fiber degeneration, or additional genetic variants, which might play an additive role (Mis et al., 2019) in combination with the p.(Tyr66Ser) variant studied here. Considering that patient II.2, on the other hand, did not experience spontaneous pain but showed a pathological pain response upon sine-wave stimulation, we hypothesize that while CMi-fiber pathology might be a requirement for the development of neuropathic pain, it alone might not be a sufficient explanation in a one-to-one causal relationship. Overall, QST results and pain responses to cutaneous axonal stimulation were compatible with a mixed gain- and loss-of-fiber-function phenotype in both patients.

Interestingly, gain- and loss-of-function properties were also evident at the channel protein level: as revealed by voltage-clamp recordings, the p.(Tyr66Ser) alteration resulted in robust depolarizing shifts of both the voltage dependence of channel activation and inactivation of $Na_V1.9$ by almost 17 and 14 mV, respectively, and slowed down fast channel inactivation. Consequently, the steady-state window current, which is characterized by the overlap of the activation and inactivation curves (Fig. 4 C), has also been shifted to higher potentials, predicting reduced activity of the variant at low membrane voltages and increased activity in depolarized conditions. As demonstrated by current-clamp recordings on transfected DRG neurons, the variant p.(Tyr66Ser) also affected the shape of action potential waveforms as indicated by a slightly yet significantly shorter action potential duration and a more pronounced afterhyperpolarization. A recent study suggests a significant role for $Na_V1.9$ in the upstroke and—due to its larger persistent current—for the shoulder formation of the action potential (Köster et al., 2025). Mutant channels activate at more depolarized voltages compared with the wild type (Fig. 4 B). Consequently, they contribute less to the initial rising phase of the action potential and, thus, also to the formation of the action potential shoulder during repolarization.

Although firing frequencies in response to graded current stimulations of neurons overexpressing variant p.(Tyr66Ser) tended to be reduced at low and increased at higher stimulation intensities, this trend did not reach the level of significance. One possible explanation could be that the gain- and loss-of-function properties of the variant largely compensate for each other and that additional, yet unknown factors or processes are important, which are not fully replicated in transiently transfected murine neurons. One process with the potential to substantially modulate the activity of $Na_V1.9$ and, thus, neuronal excitability is phosphorylation. Previous studies have established that $Na_V1.9$ is highly regulated by inflammatory mediators, such as prostaglandins or nerve growth factors, which typically act via G protein–coupled receptors that trigger phosphorylation (Baker et al., 2003; Rush and Waxman, 2004; Ostman et al., 2008; Maingret et al., 2008). Interestingly, p.(Tyr66Ser) in $Na_V1.9$ is part of a phosphorylation consensus sequence that is conserved across various Na_V subtypes and is predicted to be a target of Fyn kinase. Fyn belongs to the Src family of nonreceptor kinases and plays a role in various neurological processes, including myelination, neurodevelopment, and neuroinflammatory responses (Knox and Jiang, 2015; Krämer-Albers and White, 2011). Furthermore, Fyn-dependent phosphorylation of the conserved tyrosine has been demonstrated in $Na_V1.2$ (Tyr.66) and $Na_V1.5$ (Tyr.68), where it interferes with channel inactivation (Beacham et al., 2007; Iqbal et al., 2018). Equally important, the p.(Tyr66Ser) alteration in $Na_V1.9$ does not only remove a potential target site of Fyn, but is also predicted to generate a potential consensus site for protein kinase A (PKA)–dependent phosphorylation (NetPhos 3.1) (Blom et al., 1999), potentially leading to dysregulation of the variant by PKA-dependent pathways that have a well-documented role in inflammatory pain responses and sensory sensitization (Basbaum et al., 2009; Hucho and Levine, 2007).

Despite *SCN11A* being a strong candidate gene to be involved in the development of SFN, the specific gene–disease relationship is not yet fully understood. In a unique way, this study provides in-depth clinical and paraclinical characterization and functional measurements at the fiber and channel level, and, for the first time, sheds light on the longitudinal course and short-term prognosis of a rare sodium channelopathy based on a 5-year prospective follow-up. The main limitation of this study is the *n-of-two* character, not allowing for profound statistical conclusions on effect sizes or extrapolatability in larger cohorts. However, this is a common problem in ultra-rare diseases, where patients may be excluded from potentially effective treatment options or participation in clinical trials due to sample size.

In our network, we dedicate a specific research focus to the investigation of these very rare variant–disease relationships, aiming for individualized treatment strategies in the future. Another limitation is that for cosegregation studies, our pedigree comprises two adjacent generations only so that formally, variant transmission occurred with a probability of 50%, independent from pathogenicity. The genotype–phenotype correlation is

Downloaded from rupress.org/jgp/article-pdf/157/6/e202413691/1952150/jgp_202413691.pdf by guest on 15 November 2026

still meaningful, however, but should be interpreted with caution.

As a particular strength of this study, our results arise from an interdisciplinary network and example of how urgently clinical, genetic, and functional studies need to be conjoined in order to solve rare disease cases.

In summary, we identified the novel, heterozygous *SCN11A* variant p.(Tyr66Ser) in two affected individuals from the same family, who both exhibited an SFN phenotype of otherwise unknown cause. The variant affects a conserved amino acid position and has not been found in healthy controls. Functional studies in murine DRG neurons demonstrated a shift in both activation and inactivation thresholds, pointing toward a combined gain- and loss-of-channel-function. This effect might clinically translate into the observed dysfunction of Aδ-and C-nerve fibers, as longitudinally assessed and quantified in the two variant carriers here. Interpreting the variant according to the pathogenicity criteria of the American College of Human Genetics (Richards et al., 2015), the overall clinical, genetic, and experimental evidence suggests classifying it as likely pathogenic (PS3, PM2, PP1). Having ruled out any other known acquired and hereditary causes of SFN, we strongly believe that the novel variant p.(Tyr66Ser) is a major contributor to the phenotype.

Data availability

Original data are available upon reasonable request to the corresponding author.

Acknowledgments

Jeanne M. Nerbonne served as editor.

We thank the patients for participating in our study. We thank Annie Calonec for conducting the axonal stimulation and pain ratings.

Angelika Lampert, Barbara Namer, Ingo Kurth, Maike F. Dohrn, and Roman Rolke have received a grant from the Interdisciplinary Centre for Clinical Research within the Faculty of Medicine at the RWTH Aachen University (TN1-1/IA 532001, TN1-2/IA 532002, TN1-6/IA 532006, IZKF TN1-9/IA 532009). Angelika Lampert, Ingo Kurth, and Roman Rolke have been funded by the BMBF consortium "Bio2Treat" (German Federal Ministry of Education and Research/Bundesministerium für Bildung und Forschung, BMBF, "Chronische Schmerzen—Innovative medizintechnische Lösungen zur Verbesserung von Prävention, Diagnostik und Therapie," contract number 13 GW0334B). Ingo Kurth and Angelika Lampert are supported by the DFG (KU 1587/6-1, KU 1587/9-1, KU 1587/10-1, KU 1587/11-1, 363055819/GRK2415 [Angelika Lampert], 368482240/GRK2416 [Angelika Lampert], LA 2740/6-1 [Angelika Lampert]). Ingo Kurth receives funding from the European Union's Horizon 2020 research and innovation program under the EJP RD COFUND-EJP N° 825575. Enrico Leipold and Samuel Kuehs have been funded by the Deutsche Forschungsgemeinschaft (DFG, LE 2338/3-2). Joachim Weis has been funded by Deutsche Forschungsgemeinschaft (DFG, WE 1406/17-1). Barbara Namer is supported by the Deutsche Forschungsgemeinschaft DFG NA 970 7-1.

Author contributions: Noortje W.M. van den Braak: conceptualization, data curation, formal analysis, investigation, project administration, resources, validation, visualization, and writing—original draft, review, and editing. Samuel Kuehs: conceptualization, data curation, formal analysis, investigation, and validation. Greta Z. Peschke: data curation, formal analysis, investigation, project administration, visualization, and writing—original draft, review, and editing. Barbara Namer: formal analysis, methodology, supervision, and writing—review and editing. Annette Lischka: investigation and writing—review and editing. Katja Eggermann: investigation and writing—review and editing. Christina Dumke: resources and writing—review and editing. Vishal S.B. Eswaran: investigation, methodology, and visualization. Stefan Nikolin: resources. Joachim Weis: investigation, resources, and validation. Jörg Bernhard Schulz: resources, supervision, and writing—review and editing. Angelika Lampert: conceptualization, funding acquisition, project administration, resources, supervision, and writing—review and editing. Ingo Kurth: conceptualization, data curation, and writing—review and editing. Roman Rolke: conceptualization, data curation, formal analysis, investigation, project administration, resources, supervision, validation, visualization, and writing—review and editing. Enrico Leipold: conceptualization, data curation, formal analysis, funding acquisition, investigation, resources, visualization, and writing—original draft, review, and editing. Maike F. Dohrn: conceptualization, data curation, formal analysis, funding acquisition, investigation, methodology, project administration, resources, supervision, validation, and writing—review and editing.

Disclosures: A. Lampert reported personal fees from Grünenthal during the conduct of the study. R. Rolke reported personal fees from Aristo Pharma, Avextra, Cannamedical, Grünenthal, Tilray Germany, and EISAI outside the submitted work; and being cospeaker of the physicians´ section of the German Association of Palliative Medicine. M.F. Dohrn reported personal fees from AstraZeneca, Alnylam, Pfizer, and Applied Therapeutics outside the submitted work. No other disclosures were reported.

Submitted: 12 October 2024
Revised: 6 February 2025
Revised: 12 April 2025
Accepted: 11 September 2025

References

Alves-Simões, M., L. Teege, C. Tomni, M. Lürkens, A. Schmidt, F. Iseppon, Q. Millet, S. Kühs, I. Katona, J. Weis, et al. 2024. NaV1.8/NaV1.9 double deletion mildly affects acute pain responses in mice. *Pain*. 166:773–792. https://doi.org/10.1097/j.pain.0000000000003411

Baker, M.D., S.Y. Chandra, Y. Ding, S.G. Waxman, and J.N. Wood. 2003. GTP-induced tetrodotoxin-resistant Na^+ current regulates excitability in mouse and rat small diameter sensory neurones. *J. Physiol.* 548:373–382. https://doi.org/10.1113/jphysiol.2003.039131

Basbaum, A.I., D.M. Bautista, G. Scherrer, and D. Julius. 2009. Cellular and molecular mechanisms of pain. *Cell*. 139:267–284. https://doi.org/10.1016/j.cell.2009.09.028

Beacham, D., M. Ahn, W.A. Catterall, and T. Scheuer. 2007. Sites and molecular mechanisms of modulation of $Na_V1.2$ channels by Fyn tyrosine

Downloaded from rupress.org/jgp/article-pdf/157/6/e202413691/1952150/jgp_202413691.pdf by guest on 15 November 2026

kinase. *J. Neurosci.* 27:11543–11551. https://doi.org/10.1523/JNEUROSCI.1743-07.2007

Bickel, A., H.H. Krämer, M.J. Hilz, F. Birklein, B. Neundörfer, and M. Schmelz. 2002. Assessment of the neurogenic flare reaction in small-fiber neuropathies. *Neurology*. 59:917–919. https://doi.org/10.1212/wnl.59.6.917

Blom, N., S. Gammeltoft, and S. Brunak. 1999. Sequence and structure-based prediction of eukaryotic protein phosphorylation sites. *J. Mol. Biol.* 294: 1351–1362. https://doi.org/10.1006/jmbi.1999.3310

Castoro, R., M. Simmons, V. Ravi, D. Huang, C. Lee, J. Sergent, L. Zhou, and J. Li. 2018. *SCN11A* Arg225Cys mutation causes nociceptive pain without detectable peripheral nerve pathology. *Neurol. Genet*. 4:e255. https://doi.org/10.1212/NXG.0000000000000255

Cummins, T.R., J.R. Howe, and S.G. Waxman. 1998. Slow closed-state inactivation: A novel mechanism underlying ramp currents in cells expressing the hNE/PN1 sodium channel. *J. Neurosci.* 18:9607–9619. https://doi.org/10.1523/JNEUROSCI.18-23-09607.1998

Devigili, G., V. Tugnoli, P. Penza, F. Camozzi, R. Lombardi, G. Melli, L. Broglio, E. Granieri, and G. Lauria. 2008. The diagnostic criteria for small fibre neuropathy: From symptoms to neuropathology. *Brain.* 131:1912–1925. https://doi.org/10.1093/brain/awn093

Dib-Hajj, S.D., J.S. Choi, L.J. Macala, L. Tyrrell, J.A. Black, T.R. Cummins, and S.G. Waxman. 2009. Transfection of rat or mouse neurons by biolistics or electroporation. *Nat. Protoc.* 4:1118–1126. https://doi.org/10.1038/nprot.2009.90

Dib-Hajj, S.D., T.R. Cummins, J.A. Black, and S.G. Waxman. 2010. Sodium channels in normal and pathological pain. *Annu. Rev. Neurosci.* 33: 325–347. https://doi.org/10.1146/annurev-neuro-060909-153234

Dohrn, M.F., C. Dumke, T. Hornemann, S. Nikolin, A. Lampert, V. Espenkott, J. Vollert, A. Ouwenbroek, M. Zanella, J.B. Schulz, et al. 2022. Deoxy-sphingolipids, oxidative stress, and vitamin C correlate with qualitative and quantitative patterns of small fiber dysfunction and degeneration. *Pain*. 163:1800–1811. https://doi.org/10.1097/j.pain.0000000000002580

Ebbinghaus, M., L. Tuchscherr, G. Segond von Banchet, L. Liebmann, V. Adams, M. Gajda, C.A. Hübner, I. Kurth, and H.-G. Schaible. 2020. Gain-of-function mutation in SCN11A causes itch and affects neurogenic inflammation and muscle function in Scn11a+/L799P mice. *PLoS One*. 15: e0237101. https://doi.org/10.1371/journal.pone.0237101

Freynhagen, R., T.R. Tölle, U. Gockel, and R. Baron. 2016. The painDETECT project - far more than a screening tool on neuropathic pain. *Curr. Med. Res. Opin.* 32:1033–1057. https://doi.org/10.1185/03007995.2016.1157460

Goodwin, G., and S.B. McMahon. 2021. The physiological function of different voltage-gated sodium channels in pain. *Nat. Rev. Neurosci.* 22:263–274. https://doi.org/10.1038/s41583-021-00444-w

de Greef, B.T.A., J.G.J. Hoeijmakers, C.M.L. Gorissen-Brouwers, M. Geerts, C.G. Faber, and I.S.J. Merkies. 2018. Associated conditions in small fiber neuropathy - a large cohort study and review of the literature. *Eur. J. Neurol.* 25:348–355. https://doi.org/10.1111/ene.13508

Han, C., Y. Yang, R.H. Te Morsche, J.P.H. Drenth, J.M. Politei, S.G. Waxman, and S.D. Dib-Hajj. 2017. Familial gain-of-function Nav1.9 mutation in a painful channelopathy. *J. Neurol. Neurosurg. Psychiatry*. 88:233–240. https://doi.org/10.1136/jnnp-2016-313804

Hansen, N., A.-K. Kahn, D. Zeller, Z. Katsarava, C. Sommer, and N. Üçeyler. 2015. Amplitudes of pain-related evoked potentials are useful to detect small fiber involvement in painful mixed fiber neuropathies in addition to quantitative sensory testing - an electrophysiological study. *Front. Neurol.* 6:244. https://doi.org/10.3389/fneur.2015.00244

Herzog, R.I., T.R. Cummins, F. Ghassemi, S.D. Dib-Hajj, and S.G. Waxman. 2003. Distinct repriming and closed-state inactivation kinetics of Nav1.6 and Nav1.7 sodium channels in mouse spinal sensory neurons. *J. Physiol.* 551:741–750. https://doi.org/10.1113/jphysiol.2003.047357

Huang, J., C. Han, M. Estacion, D. Vasylyev, J.G.J. Hoeijmakers, M.M. Gerrits, L. Tyrrell, G. Lauria, C.G. Faber, S.D. Dib-Hajj, et al. 2014. Gain-of-function mutations in sodium channel Na(v)1.9 in painful neuropathy. *Brain*. 137:1627–1642. https://doi.org/10.1093/brain/awu079

Hucho, T., and J.D. Levine. 2007. Signaling pathways in sensitization: Toward a nociceptor cell biology. *Neuron*. 55:365–376. https://doi.org/10.1016/j.neuron.2007.07.008

Iqbal, S.M., M. Aufy, W. Shabbir, and R. Lemmens-Gruber. 2018. Identification of phosphorylation sites and binding pockets for modulation of Na_v 1.5 channel by Fyn tyrosine kinase. *FEBS J.* 285:2520–2530. https://doi.org/10.1111/febs.14496

Jonas, R., B. Namer, L. Stockinger, K. Chisholm, M. Schnakenberg, G. Landmann, M. Kucharczyk, C. Konrad, R. Schmidt, R. Carr, et al. 2018. Tuning in C-nociceptors to reveal mechanisms in chronic neuropathic pain. *Ann. Neurol.* 83:945–957. https://doi.org/10.1002/ana.25231

Jumper, J., R. Evans, A. Pritzel, T. Green, M. Figurnov, O. Ronneberger, K. Tunyasuvunakool, R. Bates, A. Žídek, A. Potapenko, et al. 2021. Highly accurate protein structure prediction with AlphaFold. *Nature*. 596: 583–589. https://doi.org/10.1038/s41586-021-03819-2

Kabata, R., H. Okuda, A. Noguchi, D. Kondo, M. Fujiwara, K. Hata, Y. Kato, K. Ishikawa, M. Tanaka, Y. Sekine, et al. 2018. Familial episodic limb pain in kindreds with novel Nav1.9 mutations. *PLoS One*. 13:e0208516. https://doi.org/10.1371/journal.pone.0208516

King, M.K., E. Leipold, J.M. Goehringer, I. Kurth, and T.D. Challman. 2017. Pain insensitivity: Distal S6-segment mutations in NaV1.9 emerge as critical hotspot. *Neurogenetics*. 18:179–181. https://doi.org/10.1007/s10048-017-0513-9

Kleggetveit, I.P., B. Namer, R. Schmidt, T. Helås, M. Rückel, K. Ørstavik, M. Schmelz, and E. Jørum. 2012. High spontaneous activity of C-nociceptors in painful polyneuropathy. *Pain*. 153:2040–2047. https://doi.org/10.1016/j.pain.2012.05.017

Knox, R., and X. Jiang. 2015. Fyn in neurodevelopment and ischemic brain injury. *Dev. Neurosci.* 37:311–320. https://doi.org/10.1159/000369995

Köster, P.A., E. Leipold, J. Tigerholm, A. Maxion, B. Namer, T. Stiehl, and A. Lampert. 2025. Nociceptor sodium channels shape subthreshold phase, upstroke, and shoulder of action potentials. *J. Gen. Physiol.* 157: e202313526. https://doi.org/10.1085/jgp.202313526

Krämer-Albers, E.-M., and R. White. 2011. From axon–glial signalling to myelination: The integrating role of oligodendroglial Fyn kinase. *Cell Mol. Life Sci.* 68:2003–2012. https://doi.org/10.1007/s00018-010-0616-z

Leipold, E., A. Hanson-Kahn, M. Frick, P. Gong, J.A. Bernstein, M. Voigt, I. Katona, R. Oliver Goral, J. Altmüller, P. Nürnberg, et al. 2015. Cold-aggravated pain in humans caused by a hyperactive NaV1.9 channel mutant. *Nat. Commun.* 6:10049. https://doi.org/10.1038/ncomms10049

Leipold, E., L. Liebmann, G.C. Korenke, T. Heinrich, S. Giesselmann, J. Baets, M. Ebbinghaus, R.O. Goral, T. Stödberg, J.C. Hennings, et al. 2013. A de novo gain-of-function mutation in SCN11A causes loss of pain perception. *Nat. Genet.* 45:1399–1404. https://doi.org/10.1038/ng.2767

Lischka, A., K. Eggermann, C.J. Record, M.F. Dohrn, P. Laššuthová, F. Kraft, M. Begemann, D. Dey, T. Eggermann, D. Beijer, et al. 2023. Genetic landscape of congenital insensitivity to pain and hereditary sensory and autonomic neuropathies. *Brain*. 146:4880–4890. https://doi.org/10.1093/brain/awad328

Leng, X.-R., X.-H. Qi, Y.-T. Zhou, and Y.-P. Wang. 2017. Gain-of-function mutation p.Arg225Cys in SCN11A causes familial episodic pain and contributes to essential tremor. *J. Hum. Genet.* 62:641–646. https://doi.org/10.1038/jhg.2017.21

Lischka, A., P. Lassuthova, A. Çakar, C.J. Record, J. Van Lent, J. Baets, M.F. Dohrn, J. Senderek, A. Lampert, D.L. Bennett, et al. 2022. Genetic pain loss disorders. *Nat. Rev. Dis. Primers*. 8:41. https://doi.org/10.1038/s41572-022-00365-7

Lolignier, S., C. Bonnet, C. Gaudioso, J. Noël, J. Ruel, M. Amsalem, J. Ferrier, L. Rodat-Despoix, V. Bouvier, Y. Aissouni, et al. 2015. The Nav1.9 channel is a key determinant of cold pain sensation and cold allodynia. *Cell Rep.* 11:1067–1078. https://doi.org/10.1016/j.celrep.2015.04.027

Lomize, A.L., S.C. Todd, and I.D. Pogozheva. 2022. Spatial arrangement of proteins in planar and curved membranes by PPM 3.0. *Protein Sci.* 31: 209–220. https://doi.org/10.1002/pro.4219

Loose, S., A. Lischka, S. Kuehs, C. Nau, S.H. Heinemann, I. Kurth, and E. Leipold. 2023. Peripheral temperature dysregulation associated with functionally altered NaV1.8 channels. *Pflugers Arch.* 475:1343–1355. https://doi.org/10.1007/s00424-023-02856-2

Magerl, W., E.K. Krumova, R. Baron, T. Tölle, R.-D. Treede, and C. Maier. 2010. Reference data for quantitative sensory testing (QST): Refined stratification for age and a novel method for statistical comparison of group data. *Pain*. 151:598–605. https://doi.org/10.1016/j.pain.2010.07.026

Maingret, F., B. Coste, F. Padilla, N. Clerc, M. Crest, S.M. Korogod, and P. Delmas. 2008. Inflammatory mediators increase Nav1.9 current and excitability in nociceptors through a coincident detection mechanism. *J. Gen. Physiol.* 131:211–225. https://doi.org/10.1085/jgp.200709935

Makar, G., S. Kahlon, and M. Seeley. 2023. Congenital insensitivity to pain due to a de novo L369P mutation in the SCN11A gene with heterotrophic ossification - A case report. *J. Orthop. Case Rep.* 13:19–23. https://doi.org/10.13107/jocr.2023.v13.i08.3798

Matsubara, Y., H. Okuda, K.H. Harada, S. Youssefian, and A. Koizumi. 2021. Mechanical allodynia triggered by cold exposure in mice with the Scn11a p.R222S mutation: A novel model of drug therapy for neuropathic pain

Downloaded from rupress.org/jgp/article-pdf/157/6/e202413691/1952150/jgp_202413691.pdf by guest on 15 November 2026

related to NaV1.9. *Naunyn. Schmiedebergs. Arch. Pharmacol.* 394:299–306. https://doi.org/10.1007/s00210-020-01978-z

Meents, J.E., E. Bressan, S. Sontag, A. Foerster, P. Hautvast, C. Rösseler, M. Hampl, H. Schüler, R. Goetzke, T.K.C. Le, et al. 2019. The role of Nav1.7 in human nociceptors: Insights from human induced pluripotent stem cell-derived sensory neurons of erythromelalgia patients. *Pain*. 160: 1327–1341. https://doi.org/10.1097/j.pain.0000000000001511

Mis, M.A., Y. Yang, B.S. Tanaka, C. Gomis-Perez, S. Liu, F. Dib-Hajj, T. Adi, R. Garcia-Milian, B.R. Schulman, S.D. Dib-Hajj, and S.G. Waxman. 2019. Resilience to pain: A peripheral component identified using induced pluripotent stem cells and dynamic clamp. *J. Neurosci.* 39:382–392. https://doi.org/10.1523/JNEUROSCI.2433-18.2018

Nagao, C., H. Okuda, G.-J. Bekker, A. Noguchi, T. Takahashi, A. Koizumi, S. Youssefian, T. Tezuka, and S. Akioka. 2025. Familial episodic pain syndrome: A Japanese family harboring the novel variant c.2431C>T (p.Leu811Phe) in SCN11A. *Biochem. Genet.* 63:3584–3599. https://doi.org/10.1007/s10528-024-10888-1

Namer, B., and H.O. Handwerker. 2009. Translational nociceptor research as guide to human pain perceptions and pathophysiology. *Exp. Brain Res.* 196:163–172. https://doi.org/10.1007/s00221-009-1777-6

Ochoa, J.L., M. Campero, J. Serra, and H. Bostock. 2005. Hyperexcitable polymodal and insensitive nociceptors in painful human neuropathy. *Muscle Nerve*. 32:459–472. https://doi.org/10.1002/mus.20367

Okuda, H., A. Noguchi, H. Kobayashi, D. Kondo, K.H. Harada, S. Youssefian, H. Shioi, R. Kabata, Y. Domon, K. Kubota, et al. 2016. Infantile pain episodes associated with novel Nav1.9 mutations in familial episodic pain syndrome in Japanese families. *PLoS One*. 11:e0154827. https://doi.org/10.1371/journal.pone.0154827

Ostman, J.A.R., M.A. Nassar, J.N. Wood, and M.D. Baker. 2008. GTP up-regulated persistent Na^+ current and enhanced nociceptor excitability require NaV1.9. *J. Physiol.* 586:1077–1087. https://doi.org/10.1113/jphysiol.2007.147942

Peters, M.J.H., M. Bakkers, I.S.J. Merkies, J.G.J. Hoeijmakers, E.P.M. van Raak, and C.G. Faber. 2013. Incidence and prevalence of small-fiber neuropathy: A survey in The Netherlands. *Neurology*. 81:1356–1360. https://doi.org/10.1212/WNL.0b013e3182a8236e

Pettersen, E.F., T.D. Goddard, C.C. Huang, E.C. Meng, G.S. Couch, T.I. Croll, J.H. Morris, and T.E. Ferrin. 2021. UCSF ChimeraX: Structure visualization for researchers, educators, and developers. *Protein Sci.* 30:70–82. https://doi.org/10.1002/pro.3943

Phatarakijnirund, V., S. Mumm, W.H. McAlister, D.V. Novack, D. Wenkert, K.L. Clements, and M.P. Whyte. 2016. Congenital insensitivity to pain: Fracturing without apparent skeletal pathobiology caused by an autosomal dominant, second mutation in SCN11A encoding voltage-gated sodium channel 1.9. *Bone*. 84:289–298. https://doi.org/10.1016/j.bone.2015.11.022

Richards, S., N. Aziz, S. Bale, D. Bick, S. Das, J. Gastier-Foster, W.W. Grody, M. Hegde, E. Lyon, E. Spector, et al. 2015. Standards and guidelines for the interpretation of sequence variants: A joint consensus recommendation of the American College of medical genetics and Genomics and the association for molecular pathology. *Genet. Med.* 17:405–424. https://doi.org/10.1038/gim.2015.30

Rolke, R., R. Baron, C. Maier, T.R. Tölle, D.R. Treede, A. Beyer, A. Binder, N. Birbaumer, F. Birklein, I.C. Bötefür, et al. 2006. Quantitative sensory testing in the German research network on neuropathic pain (DFNS): Standardized protocol and reference values. *Pain*. 123:231–243. https://doi.org/10.1016/j.pain.2006.01.041

Rukwied, R., C. Thomas, O. Obreja, F. Werland, I.P. Kleggetveit, E. Jorum, R.W. Carr, B. Namer, and M. Schmelz. 2020. Slow depolarizing stimuli differentially activate mechanosensitive and silent C nociceptors in human and pig skin. *Pain*. 161:2119–2128. https://doi.org/10.1097/j.pain.0000000000001912

Rush, A.M., and S.G. Waxman. 2004. PGE2 increases the tetrodotoxin-resistant Nav1.9 sodium current in mouse DRG neurons via G-proteins. *Brain Res.* 1023:264–271. https://doi.org/10.1016/j.brainres.2004.07.042

Salvatierra, J., M. Diaz-Bustamante, J. Meixiong, E. Tierney, X. Dong, and F. Bosmans. 2018. A disease mutation reveals a role for NaV1.9 in acute itch. *J. Clin. Invest.* 128:5434–5447. https://doi.org/10.1172/JCI122481

Sauerstein, K., J. Liebelt, B. Namer, R. Schmidt, R. Rukwied, and M. Schmelz. 2018. Low-frequency stimulation of silent nociceptors induces secondary mechanical hyperalgesia in human skin. *Neuroscience*. 387:4–12. https://doi.org/10.1016/j.neuroscience.2018.03.006

Siedler, G., C. Sommer, and N. Üçeyler. 2020. Pain-related evoked potentials in patients with large, mixed, and small fiber neuropathy. *Clin. Neurophysiol.* 131:635–641. https://doi.org/10.1016/j.clinph.2019.12.006

Smith, A.G., M. Lessard, S. Reyna, M. Doudova, and J.R. Singleton. 2014. The diagnostic utility of Sudoscan for distal symmetric peripheral neuropathy. *J. Diabetes Complicat.* 28:511–516. https://doi.org/10.1016/j.jdiacomp.2014.02.013

Troshin, P.V., J.B. Procter, and G.J. Barton. 2011. Java bioinformatics analysis web services for multiple sequence alignment–JABAWS:MSA. *Bioinformatics*. 27:2001–2002. https://doi.org/10.1093/bioinformatics/btr304

Varadi, M., D. Bertoni, P. Magana, U. Paramval, I. Pidruchna, M. Radhakrishnan, M. Tsenkov, S. Nair, M. Mirdita, J. Yeo, et al. 2024. AlphaFold protein structure database in 2024: Providing structure coverage for over 214 million protein sequences. *Nucleic Acids Res.* 52:D368–D375. https://doi.org/10.1093/nar/gkad1011

Weidner, W. 1999. [Alpha-blockers for treatment of chronic prostatitis in combination with antibiotics. Comment on the contribution by Barbalias et al]. *Urologe A.* 38:184. https://doi.org/10.1007/s001200050264

Weis, J., I. Katona, G. Müller-Newen, C. Sommer, G. Necula, C. Hendrich, A.C. Ludolph, and A.-D. Sperfeld. 2011. Small-fiber neuropathy in patients with ALS. *Neurology*. 76:2024–2029. https://doi.org/10.1212/WNL.0b013e31821e553a

Werland, F., R. de Col, M. Hirth, B. Turnquist, M. Schmelz, and O. Obreja. 2021. Mechanical sensitization, increased axonal excitability, and spontaneous activity in C-nociceptors after ultraviolet B irradiation in pig skin. *Pain*. 162:2002–2013. https://doi.org/10.1097/j.pain.0000000000002197

Woods, C.G., M.O.E. Babiker, I. Horrocks, J. Tolmie, and I. Kurth. 2015. The phenotype of congenital insensitivity to pain due to the NaV1.9 variant p.L811P. *Eur. J. Hum. Genet.* 23:561–563. https://doi.org/10.1038/ejhg.2014.166

Zhang, X.Y., J. Wen, W. Yang, C. Wang, L. Gao, L.H. Zheng, T. Wang, K. Ran, Y. Li, X. Li, et al. 2013. Gain-of-function mutations in SCN11A cause familial episodic pain. *Am. J. Hum. Genet.* 93:957–966. https://doi.org/10.1016/j.ajhg.2013.09.016

Zhao, C., J. Jin, H. Hu, X. Zhou, and X. Shi. 2022. The gain-of-function R222S variant in *Scn11a* contributes to visceral hyperalgesia and intestinal dysmotility in *Scn11a* $^{R222S/R222S}$ mice. *Front Neurol.* 13:856459. https://doi.org/10.3389/fneur.2022.856459

Downloaded from rupress.org/jgp/article-pdf/157/6/e202413691/1952150/jgp_202413691.pdf by guest on 15 November 2026

Supplemental material

Downloaded from rupress.org/jgp/article-pdf/157/6/e202413691/1952150/jgp_202413691.pdf by guest on 15 November 2026

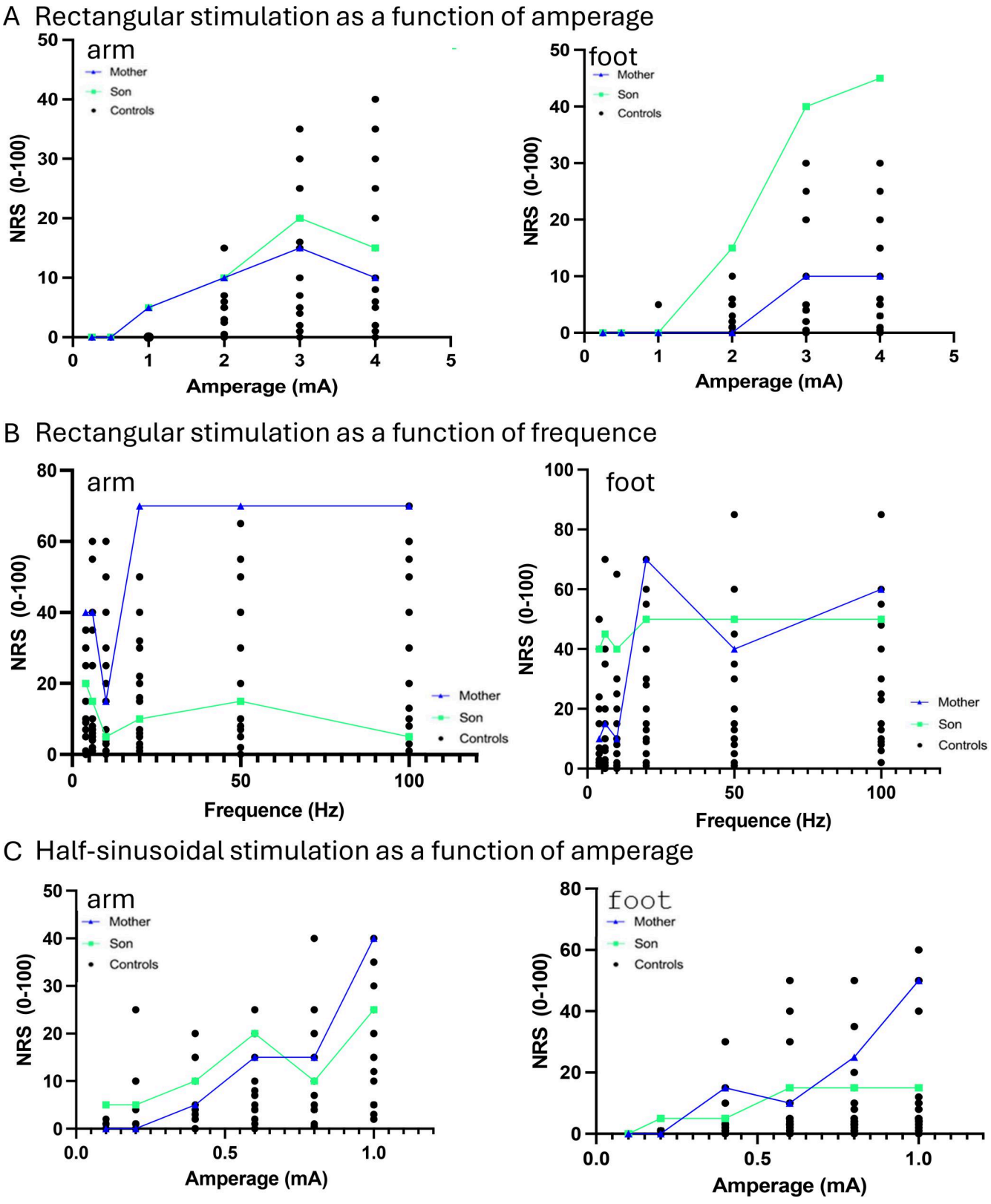


Figure S1. **Rectangular and half-sinusoidal axon stimulation.** Pain intensity ratings on the NRS 0–100 during axon stimulation for the mother (blue), son (green), and 20 controls (black). **(A–C)** Two stimulations sites, arm (leftside of the figure) and foot dorsum (rightside of the figure), are being juxtaposed for rectangular stimulation as a function of amperage (A) and frequency (B), half-sinusoidal stimulation as a function of amperage (C).

Downloaded from rupress.org/jgp/article-pdf/157/6/e202413691/1952150/jgp_202413691.pdf by guest on 15 November 2026

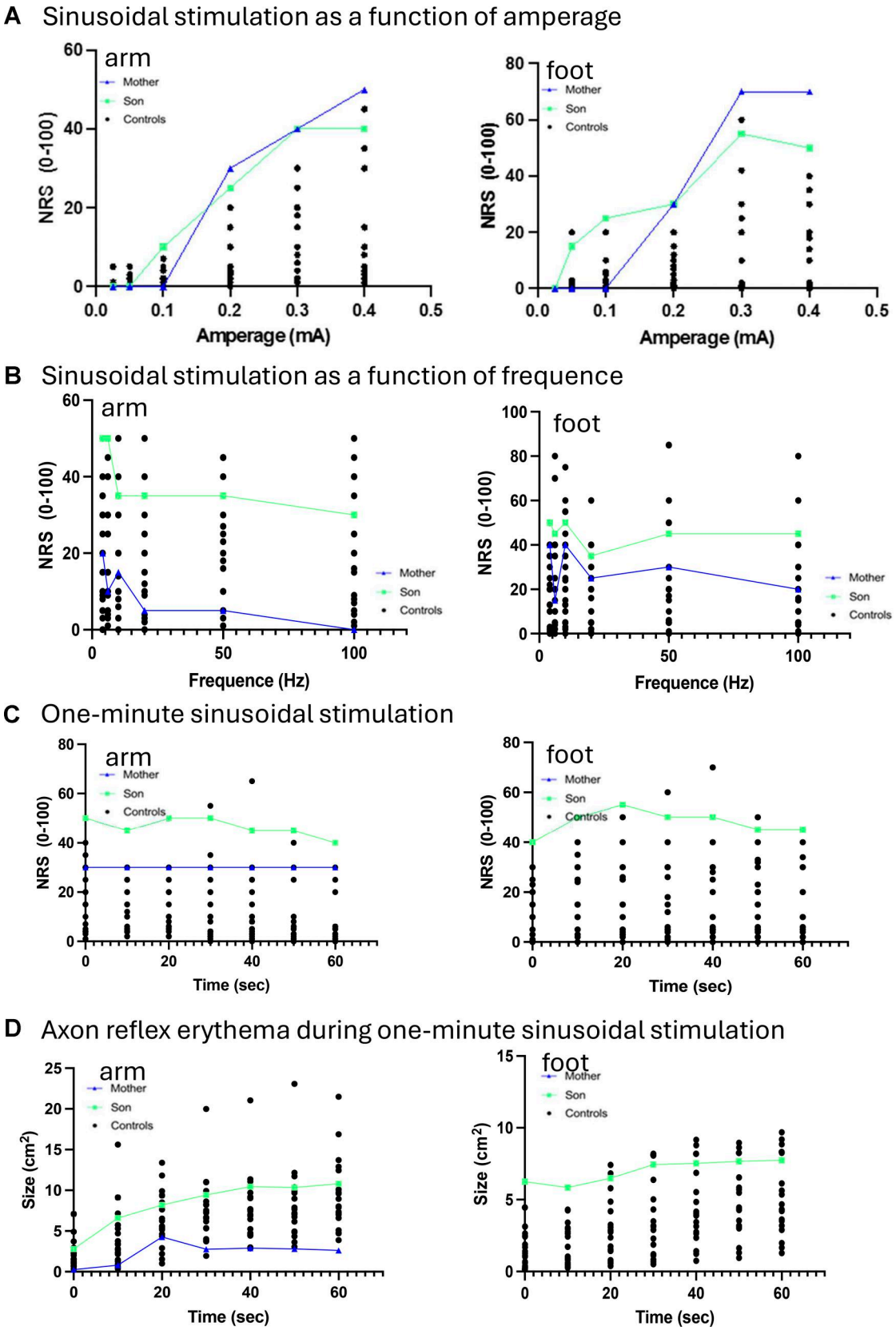


Figure S2. **Sinusoidal axon stimulation. (A–D)** Sinusoidal stimulation as a function of amperage (A) and frequency (B), one-min sinusoidal stimulation (C), and axon reflex erythema over a 1-min stimulation period (D). Two stimulations sites, arm (leftside of the figure) and foot dorsum (rightside of the figure). Data from the mother, at the foot dorsum, were not interpretable (Fig. S2 C rightside) or too low to qualify (Fig. S2 D rightside) and were therefore not included in the figure.

Downloaded from rupress.org/jgp/article-pdf/157/6/e202413691/1952150/jgp_202413691.pdf by guest on 15 November 2026

Provided online is Table S1. Table S1 shows (Likely) pathogenic SCN11A variants and associated phenotypes.

Downloaded from rupress.org/jgp/article-pdf/157/6/e202413691/1952150/jgp_202413691.pdf by guest on 15 November 2026